

1 **Cleavage-furrow formation without F-actin in *Chlamydomonas***

2 **Masayuki Onishi<sup>a,b,1</sup>, James G. Umen<sup>c</sup>, Frederick R. Cross<sup>d</sup>, and John R. Pringle<sup>a,1</sup>**

3 <sup>a</sup> Department of Genetics, Stanford University School of Medicine, Stanford, CA 94305

4 <sup>b</sup> Department of Biology, Duke University, Durham, NC 27708

5 <sup>c</sup> Donald Danforth Plant Science Center, St. Louis, MO 63132

6 <sup>d</sup> The Rockefeller University, New York, New York 10065

7 <sup>1</sup> To whom correspondence may be addressed. Email [onishi@stanford.edu](mailto:onishi@stanford.edu);

8 [jpringle@stanford.edu](mailto:jpringle@stanford.edu)

9 **Running title:** Cleavage furrows without actin

10 **Key words:** chloroplast division; cytokinesis; microtubules; myosin

## 11 **Abstract**

12 It is widely believed that cleavage-furrow formation during cell division is driven by the  
13 contraction of a ring containing F-actin and type-II myosin. However, even in cells that have  
14 such rings, they are not always essential for furrow formation. Moreover, many taxonomically  
15 diverse eukaryotic cells divide by furrowing but have no type-II myosin, making it unlikely that  
16 an actomyosin ring drives furrowing. To explore this issue further, we have used one such  
17 organism, the green alga *Chlamydomonas reinhardtii*. We found that although F-actin is  
18 concentrated in the furrow region, none of the three myosins (of types VIII and XI) is localized  
19 there. Moreover, when F-actin was eliminated through a combination of a mutation and a drug,  
20 furrows still formed and the cells divided, although somewhat less efficiently than normal.  
21 Unexpectedly, division of the large *Chlamydomonas* chloroplast was delayed in the cells lacking  
22 F-actin; as this organelle lies directly in the path of the cleavage furrow, this delay may explain,  
23 at least in part, the delay in cell division itself. Earlier studies had shown an association of  
24 microtubules with the cleavage furrow, and we used a fluorescently tagged EB1 protein to show  
25 that at least the microtubule plus-ends are still associated with the furrows in the absence of F-  
26 actin, consistent with the possibility that the microtubules are important for furrow formation.  
27 We suggest that the actomyosin ring evolved as one way to improve the efficiency of a core  
28 process for furrow formation that was already present in ancestral eukaryotes.

## 29 **Introduction**

30 Cytokinesis is the final stage in the cell-division cycle in which the cytoplasm and plasma  
31 membranes of the daughter cells are separated. In unikonts [animals, fungi, slime molds, and  
32 their close relatives], cytokinesis occurs by the symmetric or asymmetric ingression of a  
33 "cleavage furrow" from the periphery of the cell. For 50 years, thinking about cleavage-furrow  
34 ingression in these cells has been dominated by the contractile-actomyosin-ring (CAR) model, in  
35 which bipolar filaments of myosin-II walk along actin filaments (F-actin), much as in muscle, to  
36 produce the force that pulls the plasma membrane in to form the furrow (1-4). Actin, myosin-II,  
37 and functionally related proteins are clearly present in a ring that constricts during furrow  
38 ingression in unikont cells (5-10), and there is good evidence both that this ring produces  
39 contractile force (11) and that this force is required for normal cytokinesis in at least some cell  
40 types (12-14).

41 However, there are also multiple observations that are difficult to reconcile with the CAR  
42 model, at least in its simplest forms. For example, in mammalian normal rat kidney (NRK) cells,  
43 local application of the actin-depolymerizing agent cytochalasin D to the furrow region  
44 accelerated, rather than delayed, furrowing (15, 16). Moreover, equatorial furrows could form in  
45 NRK cells while myosin-II was inhibited by blebbistatin, so long as the cells were attached to a  
46 substratum (17). Additionally, motor-impaired myosin-II was able to support a normal rate of  
47 furrow ingression in mammalian COS-7 kidney-derived cells (18). In addition, myosin-II null  
48 mutants are viable and can divide some microorganisms. In the amoeba *Dictyostelium*  
49 *discoideum* such mutants form equatorial cleavage furrows when growing on a solid substratum  
50 (19-22), and in the budding yeast *Saccharomyces cerevisiae*, the mutant cells complete division  
51 even though they fail to assemble an actin ring at the division site (9). Although cytokinesis of

52 the yeast mutants is inefficient, it can be almost completely rescued by expression of the myosin-  
53 II tail domain, which is incapable of generating force by myosin-actin interaction (23, 24). In a  
54 final example, modeling indicates that the actomyosin ring cannot provide more than a fraction  
55 of the force needed to drive furrow ingression in the face of intracellular turgor pressure in the  
56 fission yeast *Schizosaccharomyces pombe*, and pharmacological disassembly of F-actin after  
57 initiation of furrowing did not inhibit further furrow ingression (25).

58 The limitations of the CAR model become even more apparent when cytokinesis is viewed  
59 in a phylogenetic and evolutionary perspective. For example, most cells in plants divide by a  
60 mechanism (centrifugal cell-plate growth mediated by the microtubule-based phragmoplast: 26-  
61 29) that seems completely different from the cleavage-furrow ingression of unikonts, although  
62 the two groups have a common ancestor. Moreover, except for the plants, some types of algal  
63 cells, and some intracellular parasites, all non-unikont cells that have been examined divide by  
64 cleavage-furrow ingression (30-39) although they lack a myosin-II, which appears to be  
65 conserved only in the unikont lineage (40-43) [with the interesting exception of a myosin-II in  
66 the Excavate *Naegleria gruberi* (44)]. There is very little information about the mechanisms by  
67 which such furrows form, although some non-unikont cells have been reported to have actin  
68 localized in the developing furrows (33, 34, 36, 37, 45-51), raising the possibility that actin  
69 might have a role that predates and is independent of myosin-II.

70 Taken together, these and other observations (27, 52) suggest that the earliest eukaryotes  
71 [and the last eukaryotic common ancestor (LECA)] had a mechanism for cleavage-furrow  
72 formation that did not involve a CAR, although it might have involved actin. Importantly, such  
73 an ancestral mechanism could still exist as the underpinning for the seemingly diverse modes of  
74 cytokinesis seen today. To explore the nature of this postulated mechanism and the role of actin

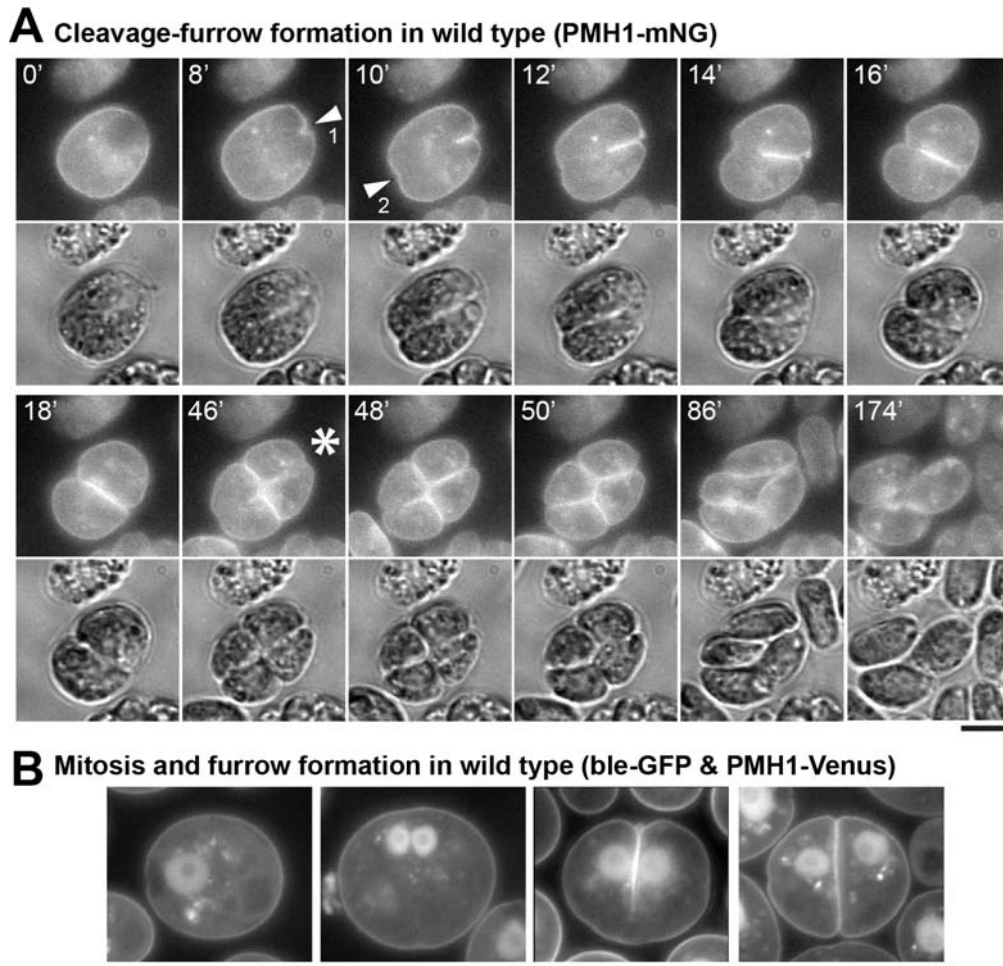
75 cytokinesis, we are studying the green alga *Chlamydomonas reinhardtii*, which divides by  
76 furrow formation (30, 53, 54; this study) but has no myosin-II (55, 56). We report here that  
77 cleavage-furrow formation in this organism does not require F-actin or any of its three non-type-  
78 II myosins. In contrast, our observations are consistent with earlier reports (30, 53, 54)  
79 suggesting a possible role for microtubules in furrow formation. Our results also suggest a  
80 previously unappreciated role for F-actin in chloroplast division.

## 81 **Results**

82 **Live-cell observations of cleavage-furrow ingression.** Previous descriptions of cytokinesis in  
83 *Chlamydomonas* have been based on light and electron micrographs of fixed cells (30, 53, 54).  
84 To observe the process in living cells, we expressed the plasma-membrane ATPase PMH1 (57)  
85 tagged with mNeonGreen (mNG) and observed cells by time-lapse microscopy. As expected,  
86 cleavage furrows ingressed primarily from one pole of each imaged cell (Fig. 1A, arrowhead 1;  
87 Movies S1 and S2); and reached the opposite side of the cell in  $16 \pm 3$  min (n=13). However, the  
88 earlier appearance of a small notch at the opposite side (Fig. 1A, arrowhead 2) suggested that a  
89 “lateral ingression” formed a groove around the entire perimeter of the plane of cleavage well  
90 before ingression of the medial furrow was complete, consistent with observations by DIC (Fig.  
91 1A, 10' and 12') and electron (30) microscopy. When the imaged cells also expressed ble-GFP (a  
92 marker for the nucleus: 58), it was apparent that the medial furrow began to form at the anterior  
93 pole of the cell and progressed between the daughter nuclei (Fig. 1B), consistent with previous  
94 reports (30, 53). In most cells, furrow ingression was accompanied by cytoplasmic rotation (Fig.  
95 1A, 0'-16').

96 Under the growth conditions used, most cells underwent two or three rapid divisions, then  
97 hatched from the mother cell wall as four or eight daughter cells (Movie S2). The second

98 cleavage followed the first by  $38 \pm 4$  min ( $n = 11$ ) and was often not clearly visible because of its  
99 angle relative to the imaging plane. However, when it could be seen clearly, it always initiated at  
100 the center of the previous cleavage (Fig. 1A, 46', asterisk; Movies S1 and S2).

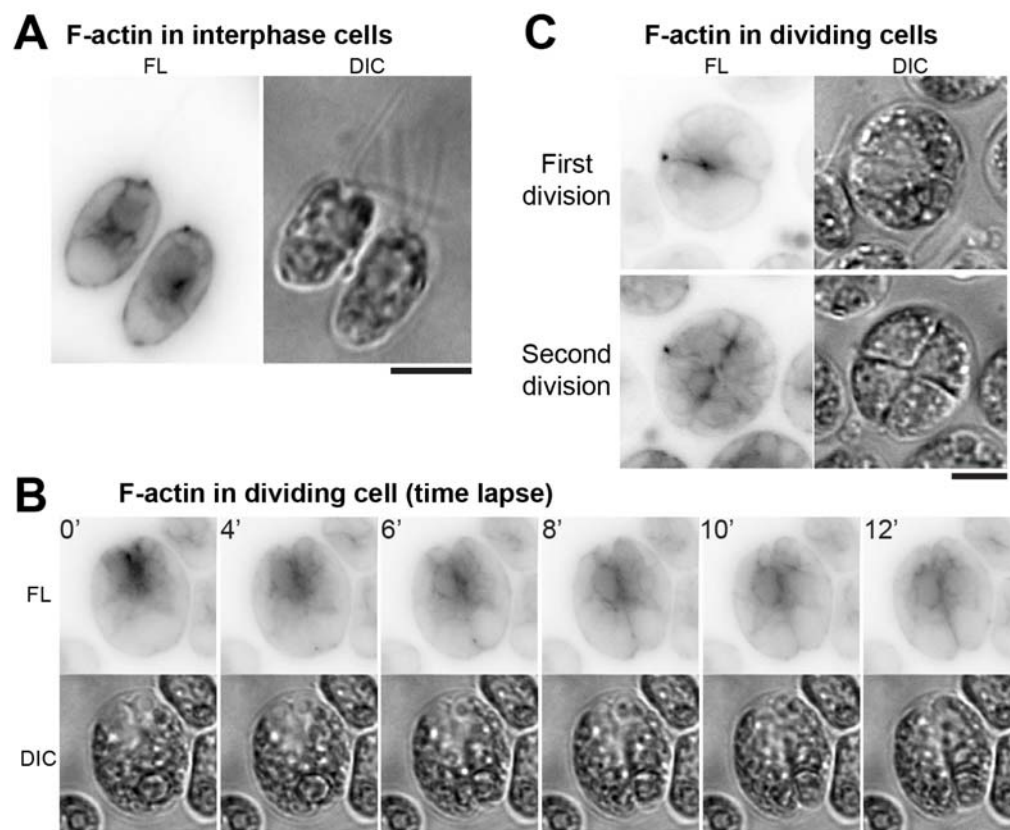


Onishi et al., Fig. 1

101

102 **Fig. 1.** Live-cell observations of cleavage-furrow formation in *Chlamydomonas*. (A) Wild-type cells  
103 expressing the plasma-membrane ATPase PMH1 tagged with mNeonGreen (mNG) were synchronized using  
104 the 12L:12D/TAP agar method, mounted on TAP + 1.5% low-melting agarose, and imaged over several hours  
105 at  $\sim 25^\circ\text{C}$ . Selected images are shown (times in min); the full series is presented in Movies S1 and S2. Upper  
106 images, mNG fluorescence (YFP channel); lower images, DIC. Arrowheads, positions of the initial  
107 appearance of furrow ingression visible in this focal plane in the anterior (1) and posterior (2) poles of the cell.  
108 Asterisk, onset of second cleavage. (B) Wild-type cells co-expressing PMH1-Venus and the nuclear marker  
109 ble-GFP were imaged using a YFP filter set during growth on TAP medium at  $26^\circ\text{C}$ . Cells at different stages  
110 in mitosis and cytokinesis are shown. Bars, 5  $\mu\text{m}$ .

111 **Localization of F-actin, but not myosins, to the cleavage furrow.** Despite the lack of a type-II  
112 myosin in *Chlamydomonas*, actin could still have a role in cleavage-furrow formation (see  
113 Introduction). To explore this possibility, we expressed the F-actin-binding peptide Lifeact (59)  
114 as a fusion with mNG. In interphase cells, F-actin localized around the nucleus, at the basal  
115 body region, and in the cortex, as observed previously (Fig. 2A; 56, 60-62). In dividing cells, F-  
116 actin showed a transient but strong enrichment at the anterior pole (Fig. 2B, 0'-4') and then  
117 appeared to be associated with the furrow throughout its ingression (Fig. 2B, 4'-12'; Fig. 2C, top).  
118 F-actin was also associated with the furrows in cells undergoing their second round of  
119 cytokinesis (Fig. 2C, bottom).



Onishi et al., Fig. 2

120

121 **Fig. 2.** F-actin localization to the region of the cleavage-furrow. Wild-type cells expressing Lifeact-mNG  
122 were imaged; fluorescence (FL) and DIC images are shown. Fluorescence images are presented with contrast



123 inverted for greater clarity. (A and C) Still images of interphase (A) and dividing (C) cells grown on TAP  
124 medium at 26°C. (B) Time-lapse images (as in Fig. 1A) showing enrichment of F-actin in the region of the  
125 cleavage furrow. Bars, 5  $\mu$ m.

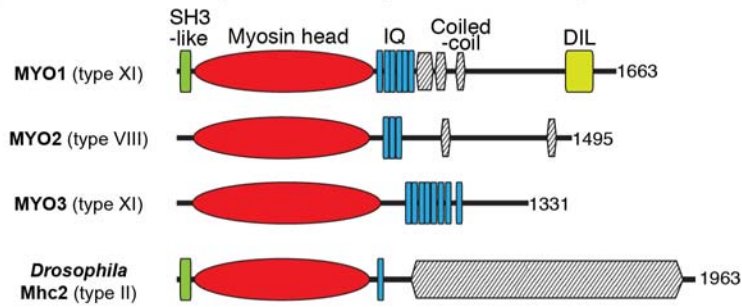
126

127 If the F-actin that concentrates in the furrow region has a role in cleavage-furrow formation,  
128 one or more myosins might also be involved. A BLAST search of the *Chlamydomonas* genome  
129 using the motor domain of *Drosophila melanogaster* type-II myosin detected only the three  
130 myosin genes reported previously (56). A phylogenetic analysis indicated that *MYO1* and *MYO3*  
131 encode type-XI myosins, whereas *MYO2* encodes a type-VIII myosin (Fig. 3A; Fig. S1A).  
132 Importantly, none of these myosins has an extended C-terminal coiled-coil domain such as those  
133 that allow type-II myosins to form bipolar filaments (63).

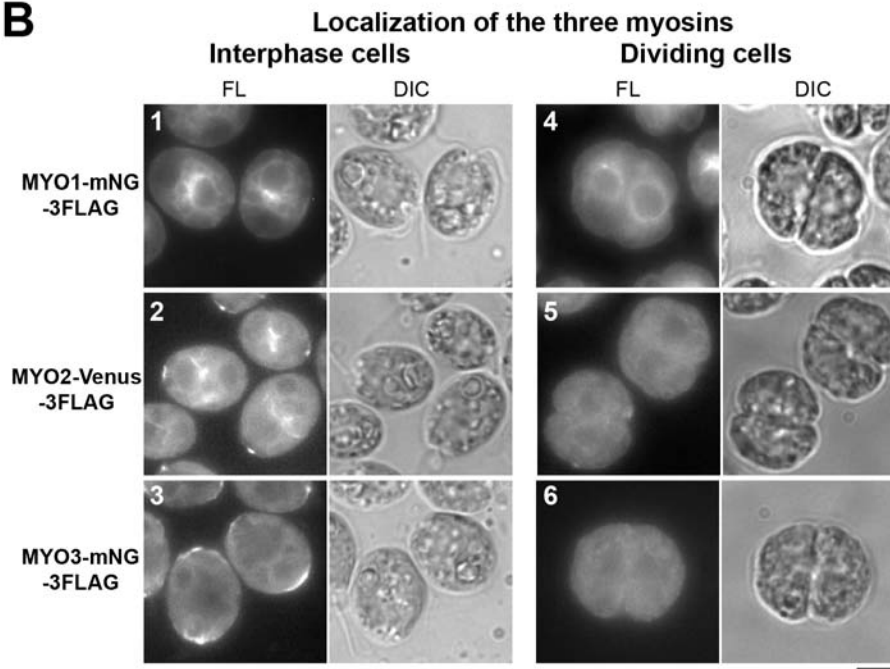
134 To ask if any of these non-type-II myosins might be involved in cytokinesis, we expressed  
135 each protein in wild-type cells with mNG-3FLAG or Venus-3FLAG fused at its C-terminus; in  
136 each case, the fusion protein was detected at or near the expected molecular weight by Western  
137 blotting (Fig. S1B). In interphase cells, *MYO1* was enriched in the perinuclear region (Fig. 3B,  
138 1; Fig. S1C, 4) in a pattern overlapping one subdomain of F-actin localization as seen with the  
139 tagged Lifeact probe (Fig. 2A; Fig. S1C, 1). *MYO2* localized to the perinuclear region as well as  
140 to dots at the cell-anterior region near the basal bodies (Fig. 3B, 2; Fig. S1C, 7), again resembling  
141 aspects of F-actin localization. *MYO3* localized to the cell-anterior region, as well as to the  
142 cortex in the cell-posterior (Fig. 3B, 3; Fig. S1C, 10). Importantly, in dividing cells, none of the  
143 myosins showed any detectable enrichment around the cleavage furrow (Fig. 3B, 4-6).



**A** The three *Chlamydomonas* myosins and a representative myosin II



**B**



Onishi et al., Fig. 3

144

145 **Fig. 3.** Lack of myosin localization to the region of the cleavage furrow. (A) Domain structures of the three  
146 *Chlamydomonas* myosins; a typical type-II myosin with a long coiled-coil tail (*Drosophila* Mhc2) is included  
147 for comparison. Domains were predicted using the HMMER (hmmer.org) and COILS (124) programs; total  
148 numbers of amino acids are indicated. (B) Localization of fluorescently tagged myosins in interphase and  
149 dividing cells; cells were grown on TAP medium at 26°C. Bar, 5  $\mu$ m.

150

151 The similarity in localization of the myosins to that of F-actin in interphase cells (see above)  
152 suggests that the tagged myosins interact normally with actin. Further evidence for this  
153 conclusion was obtained in experiments that exploited the *Chlamydomonas* system for F-actin

154 homeostasis (60, 61, 64, 65). In vegetative wild-type cells, only the conventional actin IDA5 is  
155 expressed. Exposure of cells to the F-actin-depolymerizing drug latrunculin B (LatB) leads to a  
156 rapid disassembly of F-IDA5 (Fig. S1C, 2), degradation of the monomeric IDA5, and  
157 upregulation of the divergent actin NAP1, which provides actin function by assembling into  
158 LatB-resistant filaments (Fig. S1C, 3). Similarly, the localization signals for MYO1 and MYO3  
159 were largely lost during a short incubation with LatB but subsequently recovered (Fig. S1C, 4-6  
160 and 10-12), suggesting that these tagged myosins can bind to both F-IDA5 and F-NAP1. The  
161 perinuclear signal for MYO2 was also sensitive to LatB but did not recover (Fig. S1C, 7-9; 56),  
162 suggesting that this myosin binds only to F-IDA5.

163 Thus, although the current lack of null mutations for any of the myosin genes precludes a  
164 definitive test of the function of the tagged proteins, it seems most likely that they at least  
165 localize as expected in a F-actin or NAP dependent manner, so that their apparent absence from  
166 the furrow region suggests that any function of actin in furrowing does not involve the myosins  
167 (e.g., in a noncanonical actomyosin ring).

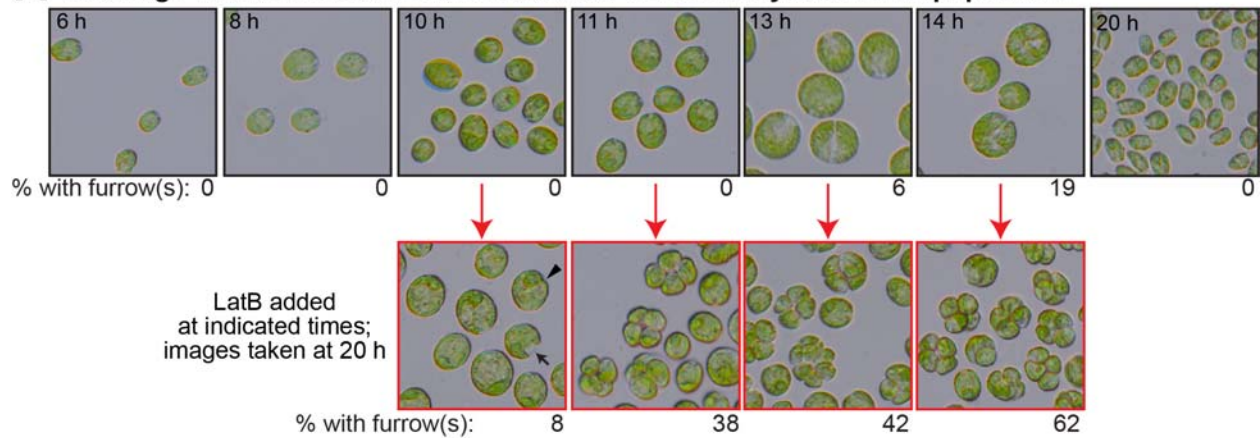
168 **Cleavage-furrow ingression in the absence of F-actin.** To ask whether actin (with or without  
169 myosin) plays a role in cleavage-furrow formation, we took advantage of our prior isolation of a  
170 null mutation (*nap1-1*) in the *NAP1* gene (60). Because F-IDA5 is highly sensitive to LatB,  
171 treatment of a *nap1-1* strain with the drug results in a rapid and complete loss of F-actin as  
172 detected by LifeAct. LatB treatment is lethal for *nap1-1* mutants, indicating that F-actin is  
173 directly or indirectly important for various cellular processes in *Chlamydomonas*. We found  
174 previously that LatB treatment of *nap1-1* cells blocked cell growth, and DNA replication and cell  
175 division were also blocked, likely as an indirect consequence of the block to cell growth. To  
176 evaluate a possible specific role of actin in cytokinesis, we employed an accurate cell-cycle

177 synchronization method using a 12:12 light-dark cycle (66, 67). Under the conditions used, the  
178 cells grew in size throughout the light phase, began to divide at ~13 h (i.e., 1 h into the dark  
179 phase), and hatched out as small daughter cells at  $\leq 20$  h (Fig. 4A, top row). We then treated  
180 aliquots of the culture with LatB at different times before and during the onset of cytokinesis and  
181 examined the cells several hours later (Fig. 4A, bottom row). When LatB was added at  $\leq 9$  h, the  
182 cells ceased growth and never detectably initiated cytokinesis. Flow-cytometry analysis in  
183 separate but similar experiments indicated that most of these cells had arrested before DNA  
184 replication as expected (60). When LatB was added at 10 h, most cells remained round and did  
185 not begin furrow formation, but a few formed what appeared to be normal cleavage furrows (Fig.  
186 4A, arrowhead) or “notch”-like structures (Fig. 4A, arrow). A similar experiment using cells  
187 expressing PMH1-Venus and ble-GFP indicated that the cells with notches had not undergone  
188 mitosis (Fig. S2A, left). In contrast, when LatB was added at  $\geq 11$  h, many cells appeared to have  
189 gone through two or more rounds of cleavage-furrow ingression, forming clusters of 4-8 cells,  
190 each of which contained a nucleus (Fig. 4A; Fig. S2A, right). In a separate but similar  
191 experiment, we noted a rough positive correlation between size of the undivided cells and their  
192 likelihood of forming a furrow in the presence of LatB (Fig. S2B), suggesting either a direct size  
193 requirement for cytokinesis or a requirement for some size-correlated cell-cycle event for actin-  
194 independent furrow formation.

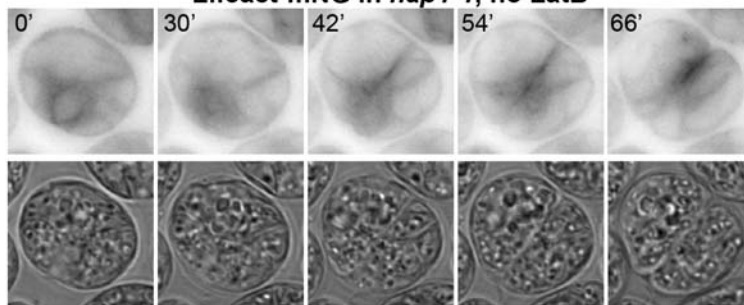
195 Although our prior work had suggested that LatB-treated *nap1-1* cells contained no residual  
196 F-actin, it seemed possible that there might be a special population of drug-resistant filaments in  
197 the cleavage-furrow region. However, no such filaments were observed when time-lapse  
198 observations were made on LatB-treated *nap1-1* cells expressing Lifeact-mNG (Fig. 4B).  
199 Moreover, consistent with our prior observations indicating rapid proteasomal degradation of

200 LatB-depolymerized IDA5 (61), IDA5 was also largely or entirely degraded by the time such  
201 cells began furrow formation (Fig. 4C).

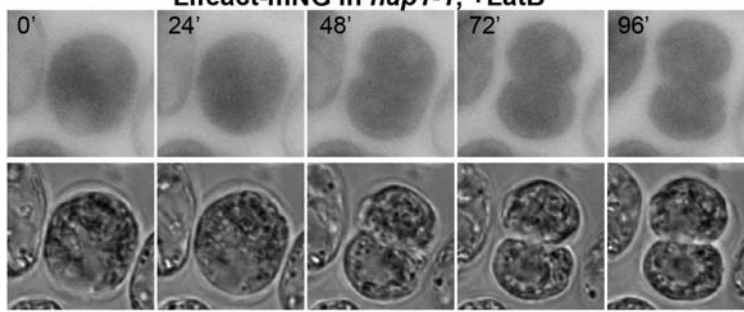
**A Cleavage-furrow formation with or without F-actin in a synchronized population**



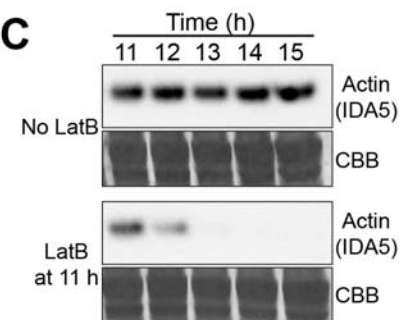
**B Lifeact-mNG in *nap1-1*, no LatB**



**Lifeact-mNG in *nap1-1*, +LatB**



**C**



202

Onishi et al., Fig. 4

203 **Fig. 4.** Cleavage-furrow formation in the absence of F-actin. (A) *nap1-1* cells were synchronized using the  
204 12L:12D/liquid TP method at 26°C, incubated for up to 20 h, and imaged at intervals (top row). At the  
205 indicated times (red arrows), samples were plated on TAP agar containing 3 μM LatB, incubated at 26°C, and  
206 then imaged at 20 h (i.e., 8 h into the dark period). The percentages of cells with visible cleavage furrows are  
207 shown below the images. (B) F-actin localization in *nap1-1* cells with or without LatB treatment. *nap1-1* cells  
208 expressing Lifeact-mNG were synchronized using the 12L:12L/TAP agar method at 26°C, mounted on TAP +  
209 1.5% low-melting agarose with or without 3 μM LatB, and observed during growth at 26°C. Selected images

210 are shown; contrast is inverted for greater clarity. The LatB-treated cell had been incubated with the drug for  
211 ~4.5 h before the first frame shown. Note that dispersion of Lifeact-mNG into the entire cytoplasm  
212 contributed to the strong apparent background in these cells. Bar, 5  $\mu\text{m}$ . (C) Rapid degradation of IDA5 upon  
213 LatB addition to a synchronized culture. *nap1-1* cells were synchronized as in (A) and the culture was split. 3  
214  $\mu\text{M}$  LatB was added to one culture at 11 h, and samples were drawn at the indicated times and subjected to  
215 Western blotting using an anti-actin antibody. 30  $\mu\text{g}$  total protein were loaded in each lane. CBB, the  
216 membrane stained with Coomassie Brilliant Blue, shown as a loading control.

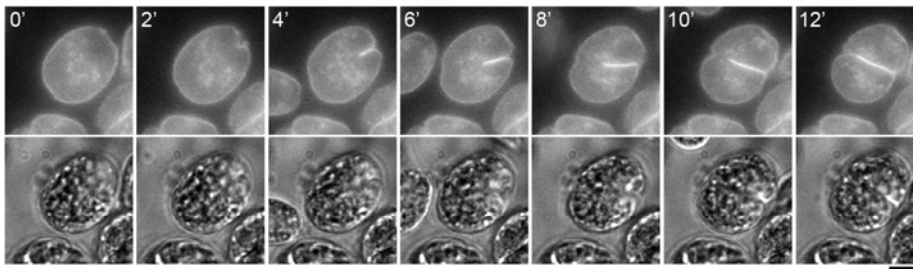
217

218 **Reduced efficiency of furrow ingression in cells lacking F-actin.** To investigate the efficiency  
219 of cleavage-furrow formation in the absence of F-actin, we performed time-lapse microscopy on  
220 *nap1-1* cells expressing PMH1-mNG. In the absence of LatB, furrow formation in these cells  
221 proceeded to completion in  $17\pm 4$  min (n=12) (Fig. 5, A and C1; Fig. S2C, 2), not significantly  
222 different from the rate in wild-type cells ( $16\pm 3$  min; n=13) (Fig. 1; Fig. 5C1; Fig. S2C, 1). In  
223 contrast, in the presence of LatB, although the rates of furrow ingression varied considerably in  
224 individual cells, they were slower in all cells examined than in control cells even during the early  
225 stages of furrow ingression, and more so during its later stages (Fig. 5B, C1, C2; Fig. S2C, 3).  
226 The time gap between the formation of a small cell-anterior notch and the detectable ingression  
227 of the medial furrow was expanded from ~2 min in control cells to 5-15 min. Moreover,  
228 although the medial furrow typically ingressed smoothly into about the middle of the cell, the  
229 second notch at the cell-posterior end did not appear normally at that time, and, in most cells, the  
230 medial furrow stalled at that point for an extended period before eventually appearing to  
231 complete its growth (10 of the 12 cells examined: Fig. 5B1, arrow; Movie S4) or regressing (one  
232 of the 12 cells examined: Fig. 5B2; Movie S5). More rarely (one of the 12 cells examined), the  
233 furrow appeared to progress across the cell without interruption (Fig. 5B3; Movie S6). In all  
234 cells examined, the daughter cells remained clustered without hatching, and the fluorescence of  
235 PMH1-mNG became quite dim, making it difficult to determine when (or whether) the plasma

236 membranes were fully resolved. Indeed, when the clusters of LatB-treated *nap1-1* cells (see Fig.  
237 4A) were treated with the cell-wall digesting enzyme autolysin, ~5% of the cells remained  
238 connected with an intercellular bridge between the pairs (Fig. S2D). Taken together, these  
239 results suggest that although actin is not required for furrow ingression per se, it plays some  
240 ancillary role(s) that facilitates the early stages of furrowing and become(s) more important  
241 during the later stages of furrow ingression and/or abscission.

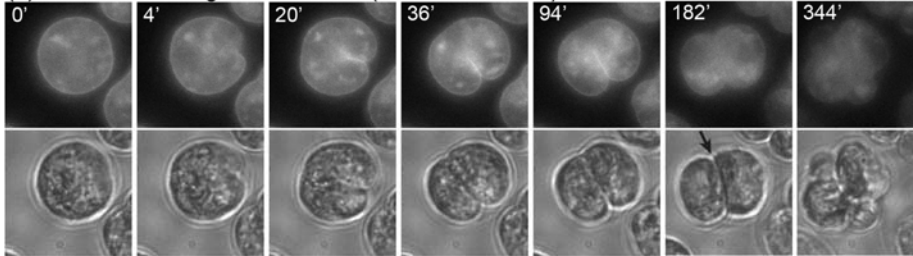


**A** Cleavage-furrow formation in *nap1-1*, no LatB (PMH1-mNG)

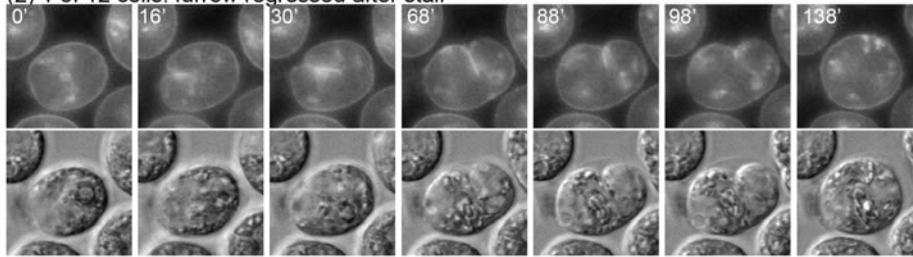


**B** Cleavage-furrow formation in *nap1-1*, +LatB (PMH1-mNG)

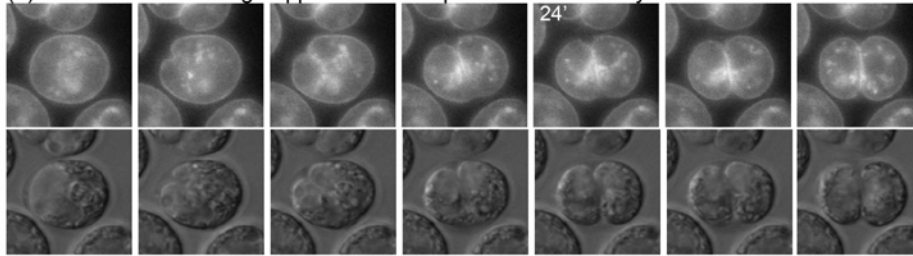
(1) 10 of 12 cells: ingress stalled (for variable times) at ~50-70%



(2) 1 of 12 cells: furrow regressed after stall

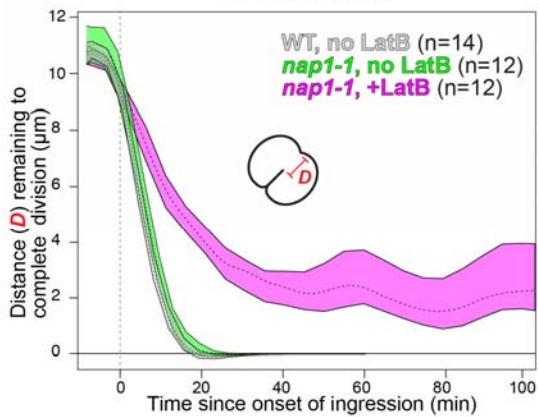


(3) 1 of 12 cells: cleavage appeared to complete with little delay

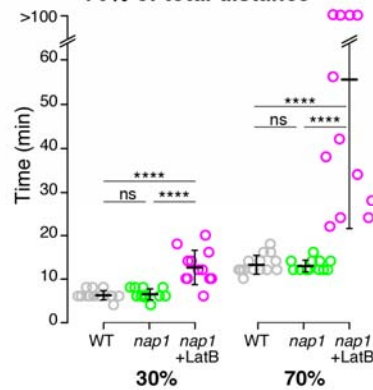


**C** Kinetics of furrow ingress with or without F-actin

1. LOESS plots



2. Time to cleave 30% or 70% of total distance



Onishi et al., Fig. 5

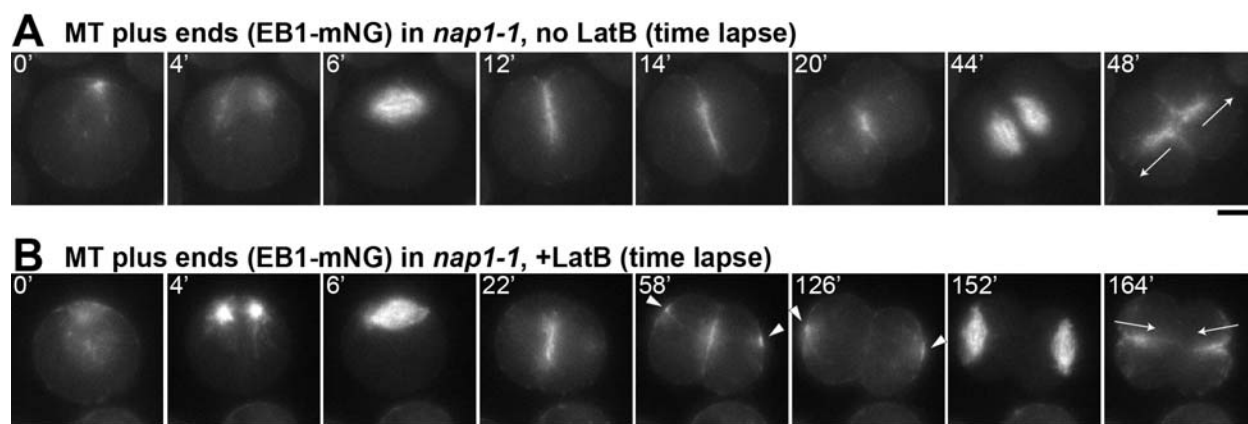


243 **Fig. 5.** Slower cleavage-furrow ingression and delay in furrow completion in the absence of F-actin. (A)  
244 *nap1-1* cells expressing PMH1-mNG were synchronized using the 12L:12D/TAP agar method and observed  
245 by time-lapse microscopy at 26°C. Full series is presented in Movie S3. Bar, 5  $\mu$ m. (B) As in A except that 3  
246  $\mu$ M LatB was added 120-160 min before the first frames shown. Selected images are shown to illustrate the  
247 different time scales; full series are presented in Movies S4-S6. Bar, 5  $\mu$ m. (C) Kinetics of furrow ingression  
248 in wild-type cells without LatB (Fig. 1A, Movie S2) and in *nap1-1* cells with or without 3  $\mu$ M LatB. Data are  
249 from the experiments shown in A and B. (1) Distance of the leading edge of the medial furrow from the  
250 opposite side of the cell as a function of time since the onset of furrow ingression (set at 0). Means and 95%  
251 confidence intervals of 1000X-bootstrapped LOESS curves are shown (see Materials and Methods). The  
252 curves for individual cells are shown in Fig. S2C. (2) Times for the furrow to reach 30% or 70% of the total  
253 distance across the cells. Because of mNG bleaching after prolonged time-lapse observations, cleavage times  
254 were capped at 100 min for these analyses. Bars indicate means and standard deviations. Statistical analyses  
255 were performed using one-way ANOVA and Tukey's post-hoc multiple comparisons (ns, not significant; \*\*\*\*,  
256  $P < 0.0001$ ).

257

258 **Association of microtubules with the cleavage furrow in the absence of F-actin.** It has long  
259 been known that microtubules (MTs) are associated with the cleavage furrows in  
260 *Chlamydomonas*, and their depolymerization by drugs or mutation largely blocks cytokinesis (30,  
261 53, 54). To ask if this association is maintained in the absence of F-actin, we first tried, but  
262 failed, to visualize the furrow-associated MTs by time-lapse imaging using a fluorescently  
263 tagged tubulin. However, we had better results upon expressing an mNG-tagged version of the  
264 plus-end-binding protein EB1 (68). In both wild-type cells (68) and *nap1-1* cells not treated with  
265 LatB (Fig. 6A, 0'; Movie S7), EB1-mNG was concentrated in the basal-body region of pre-  
266 mitotic cells. Upon entry into mitosis, EB1-mNG disappeared from the cell pole and appeared in  
267 the mitotic spindle (Fig. 6A, 4'-6'; Movie S7). After mitosis, the EB1-mNG signal reappeared at  
268 the apical pole of the cell, from which it moved into and across the cell body as the cleavage  
269 furrow formed (Fig. 6A, 12'-14'; Movie S7) and remained concentrated in the middle of the  
270 division plane after cytokinesis (Fig. 6A, 20'; Movie S7). Each daughter cell then formed an

271 EB1-labeled spindle in the region proximal to this site, and the new furrows (as marked by EB1-  
272 mNG) grew outward from the center of the cell to the surface (Fig. 6A, 44' and 48', arrows). In  
273 *nap1-1* cells treated with LatB, EB1-mNG localization was nearly normal during the first  
274 division (Fig. 6B, 0'-22'; Movie S8), except for a slower-than-normal progression through the  
275 cytoplasm, consistent with the PMH1-mNG data. However, a fraction of the EB1-mNG  
276 appeared to leave the division plane prematurely and form foci at the far sides of the daughter  
277 cells (Fig. 6B, 58'-126', arrowheads), suggesting a defect in polarity maintenance caused by the  
278 loss of F-actin. Probably as a consequence, the spindles for the second mitosis were positioned  
279 distal from the previous division plane, and the cleavage furrows subsequently grew inward (Fig.  
280 6B, 152'-164', arrows; Movie S8), although the localization of EB1-mNG, and thus presumably  
281 of both the spindle and furrow-associated MTs, otherwise appeared essentially normal. This  
282 preservation of nearly normal association of MTs with the furrows is consistent with the  
283 hypothesis that the MTs may be involved in furrow ingression both in the presence and absence  
284 of F-actin.



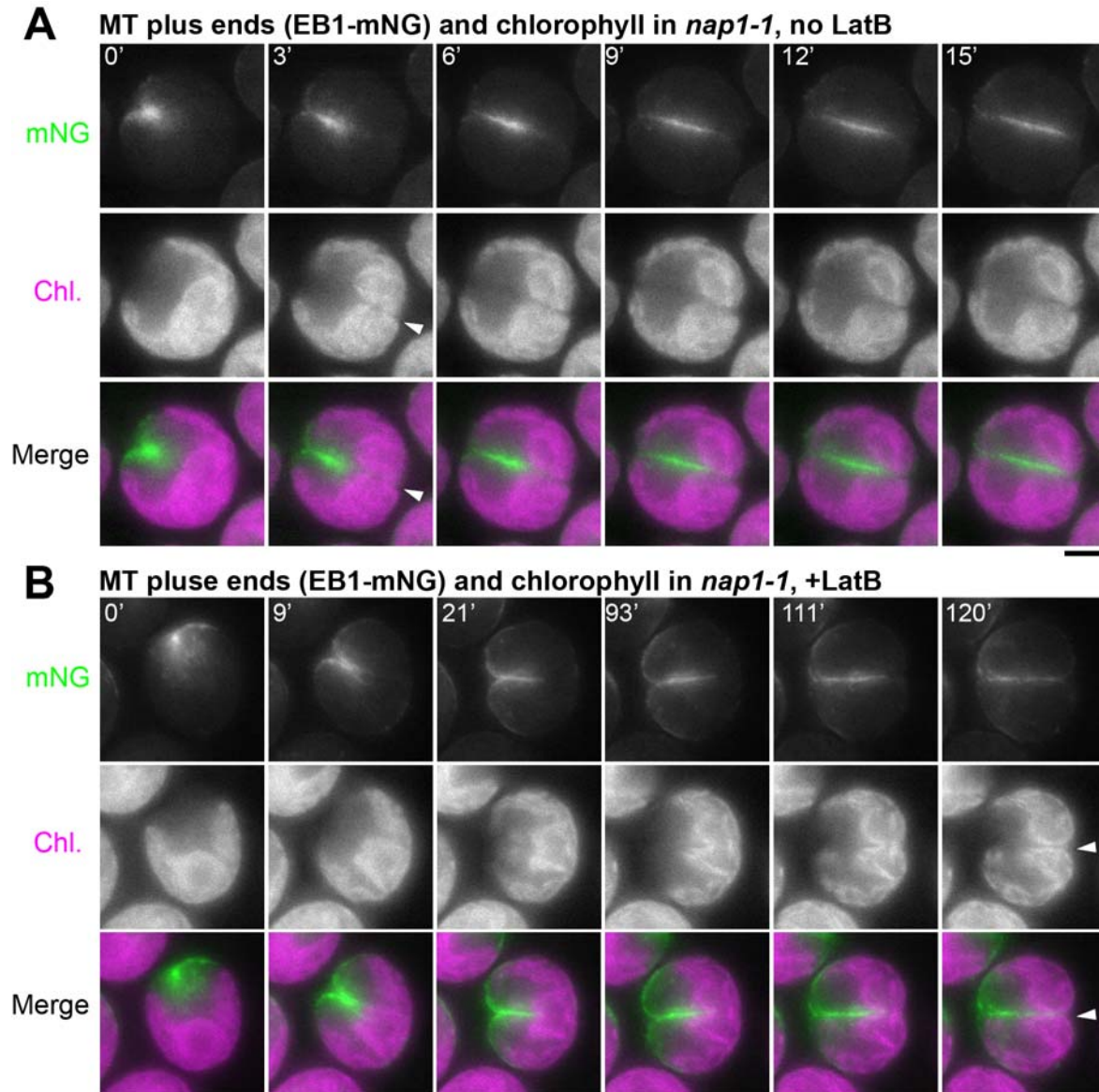
285 **Onishi et al., Fig. 6**

286 **Fig. 6.** Persistent association of microtubules with cleavage furrows, but changes in polarity during the second  
287 division, in the absence of F-actin. *nap1-1* cells expressing EB1-mNG to visualize microtubule plus ends were  
288 synchronized using the 12L:12D/TAP agar method and observed by time-lapse microscopy at 26°C. Selected

289 images are shown; full series are presented in Movies S7 and S8. (A) A cell not treated with LatB. (B) A cell  
290 treated with 3  $\mu$ M LatB beginning ~20 min before the first frame shown. Arrowheads, aberrant foci of EB1-  
291 mNG at positions distal to the cleavage furrow in cells lacking F-actin; arrows, the directions of furrowing  
292 during the second division of each cell. Bars, 5  $\mu$ m.

293

294 **Defective chloroplast division in cells without F-actin.** The EB1-mNG studies also revealed a  
295 possible cause of the delay in furrow completion in cells lacking F-actin. In normal  
296 *Chlamydomonas* cells, the large, cup-shaped chloroplast is centered on the posterior pole of the  
297 cell (Fig. 7A, 0'), so that the organelle lies squarely in the path of the ingressing cleavage furrow.  
298 In control cells, division of the chloroplast (as visualized by chlorophyll autofluorescence)  
299 appeared to have occurred by the time that the furrow (or at least its associated EB1) reached the  
300 organelle (Fig. 7A, 3', arrowhead), confirming previous observations that the chloroplast has a  
301 division machinery that is independent of, although temporally and spatially coordinated with,  
302 cleavage-furrow ingression (69, 70). In contrast, in cells lacking F-actin, the furrow appeared to  
303 partially penetrate into the undivided chloroplast over an extended period (Fig. 7B, 21'-111'),  
304 before finally moving through a gap formed in the chloroplast (Fig. 7B, arrowhead). These  
305 results suggest that efficient chloroplast division requires F-actin, that coordination of division  
306 between the cell and the plastid requires F-actin, or both, and that the physical barrier posed by  
307 the undivided chloroplast may explain the delay in furrow completion in cells lacking F-actin.



308

Onishi et al., Fig. 7

309 **Fig. 7.** Delayed chloroplast division in the absence of F-actin. EB1-mNG fluorescence and chlorophyll  
310 autofluorescence are shown in a cell not treated with LatB (A) and a cell treated with 3  $\mu$ M LatB beginning  
311 ~20 min before the first frame shown (B). Cells had been synchronized prior to imaging using the  
312 12L:12D/TAP agar method. Arrowhead, time of apparent completion of chloroplast division. Bars, 5  $\mu$ m.

### 313 Discussion

314 **Rate of cleavage-furrow ingression.** Both electron microscopy (30, 53, 71) and light  
315 microscopy (54, 72) had suggested that *Chlamydomonas* divides by means of an asymmetrically

316 ingressing cleavage furrow (67), despite its lack of a type-II myosin, and we confirmed this  
317 model by live-cell imaging using a fluorescent plasma-membrane marker. The time-lapse  
318 imaging also allowed us to determine the rate of furrow ingression. At its maximum (~0.85  
319  $\mu\text{m}/\text{min}$ ; see Fig. 5C), this rate is comparable to those in small- to medium-sized cells that have  
320 type-II myosins and form actomyosin rings at their furrow sites, such as *S. pombe* (~0.15  
321  $\mu\text{m}/\text{min}$ : 25, 73, 74), *Neurospora crassa* (1.3-3.2  $\mu\text{m}/\text{min}$ : 75), and various mammalian somatic  
322 cells (3-4  $\mu\text{m}/\text{min}$ : 18, 76-79). Thus, the presence of a CAR is not necessary to produce a rate of  
323 furrow ingression in this range.

324 **Localization of F-actin, but not myosin, to the cleavage furrow.** Our live-cell imaging also  
325 clarified the spatial relationships of the furrow, F-actin, and the three *Chlamydomonas* myosins.  
326 Although immunostaining had indicated that there was actin in the furrow region (47, 54, 65, 80),  
327 it was not clear whether this actin was in filamentous form (47). However, imaging of cells  
328 expressing the F-actin-specific probe Lifeact showed clearly that F-actin is enriched in the  
329 furrow region during most or all of the period of furrow ingression. In contrast, although a  
330 previous report had suggested (based on immunostaining with an antibody to *Dictyostelium* type-  
331 II myosin) that myosin is also localized to the furrow region (54), fluorescence tagging of the  
332 three *Chlamydomonas* myosins (two type XI and one type VIII) showed no enrichment in this  
333 region. Although this conclusion should be qualified by the lack of definitive evidence that the  
334 tagged myosins were fully functional, the loss of their localization after LatB treatment suggests  
335 that they co-localize normally with F-actin (see Results). Moreover, the likelihood of a myosin  
336 role in *Chlamydomonas* furrow formation is also reduced by our finding that F-actin itself is not  
337 essential for this process.

338 **Cleavage-furrow ingression without F-actin.** Despite the apparent absence of myosins from

339 the furrow region in *Chlamydomonas*, it seemed possible that the F-actin there might play an  
340 essential role in furrow formation. However, when we used a combination of a mutation (to  
341 eliminate the drug-resistant actin NAP1) and a drug (to depolymerize the drug-sensitive actin  
342 IDA5), the cells were still able to form cleavage furrows and divide. While it is theoretically  
343 possible that a population of drug-resistant IDA5 filaments remained specifically in the cleavage  
344 furrow, we could detect no such filaments by Lifeact staining. Moreover, Western blotting  
345 revealed that, as observed previously in asynchronous cells (61), depolymerization of F-IDA5 in  
346 dividing cells was followed quickly by degradation of IDA5 itself. Taken together, our results  
347 appear to establish that the actin cytoskeleton does not play a principal role in generating the  
348 force for cleavage-furrow ingression in *Chlamydomonas*.

349       Nonetheless, several observations indicate that actin does contribute significantly to cell  
350 division in *Chlamydomonas*. First, in the absence of F-actin, the rate of early furrow ingression  
351 was ~2-fold slower than normal. It seems possible either that actin forms a contractile structure,  
352 not dependent on myosin, that contributes some force for furrow ingression or that actin is  
353 necessary for the trafficking of Golgi-derived vesicles that ultimately provide the new cell  
354 surface material for the growing furrow. Second, the last ~30% of cleavage was slowed even  
355 more ( $\geq 5$  fold), and some cells appeared to fail (or at least have long delays in) the final  
356 abscission of the daughters. In addition, EB1 signal (marking MT plus-ends) disappeared  
357 prematurely from the furrow region when F-actin was missing, presumably reflecting a failure to  
358 maintain MT organization during the final phase of cleavage. Finally, the directions of the  
359 second cleavages were inverted, probably because the polarities of the two daughter cells  
360 produced by the first cleavage were also inverted. The precise mechanisms by which F-actin  
361 facilitates cytokinesis are not yet clear, but the observed slowness of late furrow ingression in its



362 absence appears to at least partly reflect a delay in chloroplast division (see below). Together,  
363 our findings highlight the value of using *Chlamydomonas* to explore non-CAR-related roles of  
364 the actin cytoskeleton in cytokinesis.

365 **An apparent role for F-actin in chloroplast division.** In most cells lacking F-actin, there was a  
366 delay in chloroplast division of  $\geq 120$  min. This observation was surprising, because despite  
367 early reports of an actin role in plastid division in both charophyte and red algae (81, 82), no  
368 such role has been recognized (to our knowledge) in plants or other organisms. As the  
369 *Chlamydomonas* chloroplast lies directly in the path of the ingressing cleavage furrow, the delay  
370 in chloroplast division may explain much or all of the delay also seen in furrow completion in  
371 these cells. Although we cannot currently test this model due to the lack of a method for clearing  
372 the chloroplast from the division path, a similar apparent obstruction of cytokinesis by an  
373 undivided chloroplast was observed after expression of a dominant-negative dynamin mutant in  
374 the red microalga *Cyanidioschyzon merolae* (83). Most other unicellular algae also contain only  
375 one or a few chloroplasts, whose division must presumably be coordinated both temporally and  
376 spatially (i.e., division in the same plane) with that of the cell (69). The temporal coordination is  
377 achieved, at least in part, by cell-cycle control of the expression of the proteins (such as FtsZ and  
378 dynamin) directly involved in chloroplast division (66, 84). However, the spatial coordination  
379 seems to require a local, structure-based signal. Our results suggest that the furrow-associated F-  
380 actin may provide this spatial cue to the chloroplast-division machinery and, in so doing, might  
381 also dictate the precise timing of its action.

382 **Possible role for MTs in cleavage-furrow formation.** It has long been thought that MTs may  
383 be involved in cleavage-furrow positioning and/or ingression in *Chlamydomonas*. Electron-  
384 microscopy and immunofluorescence studies have shown that two of the four "rootlet" MTs that



385 run from the basal body along the cortex align with the division plane (like the preprophase band  
386 in plant cells), while an array of many MTs, the "phycoplast", runs along the developing furrow  
387 (30, 53, 54, 85, 86). Moreover, pharmacological disruption of the MTs inhibits cytokinesis (54).  
388 Our observations on cells expressing a fluorescence-tagged EB1 protein have now added the  
389 information that dynamic MT plus-ends are associated with the furrow throughout its ingression  
390 and that this association is maintained even during furrow formation in the absence of F-actin.  
391 Thus, it seems likely that the MTs have a direct, actin-independent role in promoting furrow  
392 ingression, possibly by guiding the deposition of new cell-surface materials in the growing  
393 furrow as they do in plant-cell phragmoplasts. Testing this hypothesis and elucidating the  
394 mechanisms involved will be major goals of future studies.

395 **Cytokinesis in phylogenetic and evolutionary perspective.** Our study also sheds some light on  
396 the evolutionary origins and underlying basal mechanisms of eukaryotic cytokinesis. The wide  
397 phylogenetic distribution of division by cleavage-furrow ingression, together with the near-  
398 universal absence of myosin-II outside the unikonts, had already made clear that a conventional  
399 CAR model cannot account generally for furrow formation. Moreover, we have shown here that  
400 even F-actin is not essential for the formation of cleavage furrows in *Chlamydomonas*. This  
401 observation has some precedents and parallels. Even within the unikonts, it is clear that F-actin  
402 is not essential for furrow ingression in many cases (9, 15, 25, 87, 88; and see Introduction), and  
403 this may be the rule, rather than the exception, in non-unikonts. For example, in the ciliate  
404 *Tetrahymena pyriformis*, latrunculin A did not block cell division despite a loss of F-actin and a  
405 consequent disruption of actin-dependent processes such as food-vacuole formation (39); in the  
406 Diplomonad parasite *Giardia lamblia*, which has one actin but no myosin(38), furrowing  
407 occurred efficiently when actin expression was knocked down with a morpholino (89), although

408 the cells were delayed in abscission; and in the red alga *C. merolae*, which also has no myosin,  
409 cells divide by furrowing even though actin is not expressed under normal growth conditions  
410 (90). Taken together, these and related observations suggest that in the earliest eukaryotes, the  
411 LECA, and most branches of the modern eukaryotic phylogeny, actin and myosin are not  
412 primarily responsible for the force that produces cleavage-furrow ingression. We speculate that  
413 as prominent roles for actin and myosin evolved in the unikonts, the underlying ancestral  
414 mechanisms for driving furrow ingression may remain in force.

415 In thinking about these ancestral mechanisms, it is instructive to consider the mechanisms of  
416 cytokinesis in modern prokaryotes. Bacteria divide using a furrowing mechanism in which the  
417 tubulin-like FtsZ plays a central role (91-95), which is likely to be used also by many archaea  
418 (96-100), so the immediate prokaryotic ancestor of the first eukaryotes probably also divided by  
419 such a mechanism. Current information about FtsZ action suggests that it functions both to bend  
420 the inner membrane and to organize the symmetric deposition of cell wall, which drives in the  
421 membrane to produce the division furrow (93-95, 101). Thus, if an ancient FtsZ was the  
422 evolutionary progenitor of modern tubulin, the major role of MTs in cleavage-furrow formation  
423 in such distantly related modern eukaryotes such as *Chlamydomonas*, *G. lamblia* (89), *Penium*  
424 *margaritaceum* (102), *Trypanosoma brucei* (103), *Tetrahymena thermophila* (104), and  
425 *Toxoplasma gondii* (105) may reflect the persistence of an ancient mechanism for adding cell-  
426 surface material to form a furrow. The same interpretation might apply even to the association  
427 of parallel arrays of MTs with cleavage furrows observed in some animal cells, such as embryos  
428 of *Xenopus* (106, 107), zebrafish (108), and *Drosophila* (109), or the midbody MTs formed  
429 during metazoan abscission (27), where the MTs appear to play an important role in targeting  
430 vesicles containing new membrane. In any case, the hypothesis of a primordial role for MTs in

431 eukaryotic cytokinesis seems to make it easier to understand the central role of MTs in  
432 cytokinesis in modern plants, where both the preprophase band (which marks the future division  
433 plane) and the phragmoplast (which organizes the centrifugal deposition of new cell membrane  
434 and cell wall by fusion of post-Golgi vesicles) are MT based (29).

435 At the same time, it should also be noted that there is now good evidence that the prokaryotic  
436 ancestor of modern eukaryotes also had an actin-like protein (110, 111), and there is even some  
437 evidence that this protein might have been associated with division sites (112) despite the lack of  
438 evidence for any myosin in such organisms. Thus, the association of actin with the furrow  
439 regions both in *Chlamydomonas* and in many other eukaryotes without a myosin II may also be a  
440 preserved ancestral trait. In this regard, it is interesting that the preprophase band in plants  
441 involves actin as well as MTs, conceivably reflecting an earlier stage in plant evolution in which  
442 MTs and actin functioned together to bring about ingression of a furrow (113). If both the  
443 division mechanisms of modern plants and those of modern unikonts evolved from such an  
444 ancestral state (by recruitment of intracellular MTs to form the phragmoplast, and by reduction  
445 of the MT role in furrow formation in favor of an actomyosin system, respectively), then  
446 continuing studies of *Chlamydomonas* should help to elucidate both the two evolutionary paths  
447 and both of the modern mechanisms.

448 In summary, we suggest that a full understanding of eukaryotic cytokinesis, even in the  
449 intensively studied animal cells, will remain elusive unless a greater effort is made to incorporate  
450 the lessons about the evolution of this process that can be learned by studying it in the full  
451 diversity of modern eukaryotes.

## 452 **Materials and Methods**

453 **Strains, growth conditions, and genetic analysis.** *C. reinhardtii* wild-type strains CC-124 (mt-

454 ) and iso10 (mt+, congenic to CC-124) were the parental strains. The *nap1-1* mutant had  
455 previously been isolated and backcrossed three times in the CC-124 background (60). The ble-  
456 GFP and PMH1-Venus strains are progeny of previously established transgenic strains (57, 58,  
457 114).

458 Routine cell culture was done in Tris-acetate-phosphate (TAP) medium (115) at ~26°C  
459 under constant illumination at 50-100  $\mu\text{mol photons m}^{-2} \text{s}^{-1}$ . The same medium without acetate  
460 (TP) was used in one method for cell-cycle synchronization (see below). Except for  
461 synchronized cultures, liquid cultures were in exponential phase when experiments were  
462 performed. LatB was purchased from Adipogen (AG-CN2-0031, Lots A00143/I and A00143/J),  
463 and dilutions into TAP or TP medium were made from a 10-mM stock in DMSO. Paromomycin  
464 (Sigma or EMD Millipore) and Zeocin (InvivoGen) were used at 10  $\mu\text{g/ml}$  to select for and  
465 maintain strains that were transformed with constructs containing resistance markers.

466 Genetic crosses were performed essentially as described previously (60, 116, 117). When  
467 necessary, segregants were genotyped based on known phenotypes (LatB sensitivity, selectable  
468 marker, fluorescence, etc.) or by allele-specific PCR (60) using appropriate primers.

469 **Plasmids and transformation.** pEB1-mNG (expressing EB1 protein fused to mNeonGreen)  
470 was a kind gift from Karl Lehtreck (68). Construction of pMO431 ( $P_{HR}:MYO2\text{-CrVenus-}$   
471  $3FLAG$ ) was described previously (56); it expresses MYO2 tagged at its C-terminus with  
472 CrVenus-3FLAG from the hybrid *HSP70A/RBCS2* promoter ( $P_{HR}$ ). All other plasmids used in  
473 this study were constructed using one-step isothermal assembly (118); synthetic DNA fragments  
474 and primers were obtained from Integrated DNA Technologies. All plasmids and corresponding  
475 sequence files are available through the Chlamydomonas Resource Center  
476 (<https://www.chlamycollection.org>). pMO654 ( $P_{HR}:Lifeact\text{-mNG}$ ) was constructed by replacing

477 *CrVenus-3FLAG* in pMO459 (57) with *mNG* from pEB1-mNG. A similar replacement of  
478 *CrVenus* in pMO611 (57) with *mNG* yielded pMO665 ( $P_{HR}:mNG-3FLAG$ ), and genomic DNA  
479 sequences of the *PMHI* (Cre03.g164600), *MYO1* (Cre16.g658650), and *MYO3* (Cre13.g563800)  
480 coding regions (start codon to last coding codon, including all introns) were inserted into the  
481 *HpaI* site of pMO665 to generate pMO683 ( $P_{HR}:PMHI-mNG-3FLAG$ ), pMO668 ( $P_{HR}:MYO1-$   
482  $mNG-3FLAG$ ), and pMO669 ( $P_{HR}:MYO3-mNG-3FLAG$ ), respectively. Transformation by  
483 electroporation was done using a NEPA21 square-pulse electroporator and CHES buffer, as  
484 described previously (57), and transformants with strong Venus or mNG expression were  
485 identified by screening using a Tecan Infinite 200 PRO microplate reader at excitation and  
486 emission wavelengths of 515 and 550 nm, as described previously (57).

487 **Cell-cycle synchronization.** Three different methods were used for cell-cycle synchronization  
488 in this study: (i) the 12L:12D/liquid TP method was essentially as described by Fang et al. (119)  
489 except that TP medium at 26°C was used in place of HSM; (ii) the 12L:12D/TAP agar method  
490 was as described previously (120), except that it was carried out at 26°C; and (iii) the -N method  
491 was exactly as described previously using a combination of 21°C and 33°C (121). Although  
492 overall synchrony and the timing of mitosis and cytokinesis as determined by microscopic  
493 examination varied slightly depending on the method, we observed no significant qualitative or  
494 quantitative difference in the cells' response to F-actin perturbation introduced by LatB addition  
495 before the onset of cytokinesis.

496 **Light microscopy.** Fluorescence and DIC microscopy of cells expressing Venus-, mNG-,  
497 and/or GFP-tagged proteins was performed as follows. Cells were mounted on a thin pad of  
498 TAP medium containing 1.5% low-melting-point agarose (Invitrogen) and sealed with a  
499 coverslip and VALAP. When desired, LatB was added to the agarose-containing medium at 3

500  $\mu\text{M}$ . The cells were observed using a Nikon Eclipse 600-FN microscope equipped with an  
501 Apochromat x100/1.40 N.A. oil-immersion objective lens, an ORCA-2 cooled CCD camera  
502 (Hamamatsu Photonics), and Metamorph version 7.5 software (Molecular Devices). Signals of  
503 all fluorescent proteins were captured using YFP filters; chlorophyll autofluorescence was  
504 captured using Texas Red filters. For time-lapse experiments, the stage temperature was  
505 maintained at  $\sim 26^\circ\text{C}$  using a heater (AmScope), and the slide was continuously illuminated by  
506 red LED lights to support photosynthesis. The distance from the leading edge of the cleavage  
507 furrow to the opposite side of the cell was determined at each time point to provide an  
508 approximate quantitative measure of the progress of furrow ingression. To visualize the rates of  
509 furrow ingression, local polynomial regression curves were generated using the LOESS (locally  
510 estimated scatterplot smoothing) method, and means and 95% confidence intervals of 1000 such  
511 curves were calculated using the `loess.boot()` function in the R package `spatialEco`. Images were  
512 post-processed using ImageJ (National Institutes of Health) and Photoshop (Adobe) software.  
513 Images from a single experiment with a single strain were processed identically and can be  
514 compared directly in the Figures.

515 The bright-field images in Fig. 4A and Fig. S2D were captured using a Leica DMI 6000 B  
516 microscope equipped with a x40 objective lens and Leica DFC 450 camera. Cell-wall removal  
517 by autolysin was performed essentially as described previously (122).

518 **Western blotting.** Whole-cell extracts were prepared as described previously (61). SDS-PAGE  
519 was performed using Tris-glycine gels (8% for myosins, 11% for actin). After the proteins were  
520 transferred onto PVDF membranes, the blots were stained with a mouse monoclonal anti-FLAG  
521 (Sigma, F1804) or anti-actin (clone C4, EMD Millipore, MAB1501) antibody, followed by an  
522 HRP-conjugated anti-mouse-IgG secondary antibody (ICN Pharmaceuticals, 55564).

523 **Phylogenetic analysis.** The amino-acid sequences of all myosins in the genomes of  
524 *Chlamydomonas* (MYO1, Cre16.g658650.t1.1; MYO2, Cre09.g416250.t1.1; MYO3,  
525 Cre13.g563800.t1.1 from Phytozome v5.5: phytozome.jgi.doe.gov), *Arabidopsis thaliana* (40),  
526 *D. melanogaster* (40), and *S. cerevisiae* (Myo1, YHR023W; Myo2, YOR326W; Myo3,  
527 YKL129C; Myo4, YAL029C; Myo5, YMR109W from Saccharomyces Genome Database:  
528 [www.yeastgenome.org](http://www.yeastgenome.org)) were aligned using ClustalW 2.1 and the BLOSUM62 matrix. This  
529 alignment was then used to generate an unrooted Maximum Likelihood tree with approximate  
530 likelihood test using the VT model in PhyML (123).

531

### 532 **Acknowledgments**

533 We thank Arthur Grossman, Frej Tulin, Kresti Pecani, Geng Sa, Howard Berg, Heather  
534 Cartwright, David Ehrhardt, Takako Kato-Minoura, Ritsu Kamiya, Martin Jonikas, Luke  
535 Mackinder, Karl Lehtreck, Prachee Avasthi, Alex Paredez, and Ryuichi Nishihama for valuable  
536 discussions, the provision of valuable reagents, or both. We also thank the *Chlamydomonas*  
537 Resource Center for providing essential strains and reagents. This work was supported by  
538 National Science Foundation Grants EAGER 1548533 and MCB 1818383 (to J.R.P.), and MCB  
539 1515220 (to JGU), National Institutes of Health Grants R01GM126557 (to JGU) and  
540 5R01GM078153 (to FRC).



541 **References**

- 542 1. Schroeder TE (1968) Cytokinesis: filaments in the cleavage furrow. *Exp Cell Res*  
543 53(1):272–276.
- 544 2. Satterwhite LL, Pollard TD (1992) Cytokinesis. *Curr Opin Cell Biol* 4(1):43–52.
- 545 3. Robinson DN, Spudich JA (2004) Mechanics and regulation of cytokinesis. *Curr*  
546 *Opin Cell Biol* 16(2):182–188.
- 547 4. Eggert US, Mitchison TJ, Field CM (2006) Animal cytokinesis: from parts list to  
548 mechanisms. *Annu Rev Biochem* 75:543–566.
- 549 5. Yumura S, Mori H, Fukui Y (1984) Localization of actin and myosin for the study  
550 of ameboid movement in *Dictyostelium* using improved immunofluorescence. *J Cell*  
551 *Biol* 99(3):894–899.
- 552 6. De Lozanne A, Spudich JA (1987) Disruption of the *Dictyostelium* myosin heavy  
553 chain gene by homologous recombination. *Science* 236(4805):1086–1091.
- 554 7. Alfa CE, Hyams JS (1990) Distribution of tubulin and actin through the cell division  
555 cycle of the fission yeast *Schizosaccharomyces japonicus* var. *versatilis*: a  
556 comparison with *Schizosaccharomyces pombe*. *J Cell Sci* 96 (1):71–77.
- 557 8. Kitayama C, Sugimoto A, Yamamoto M (1997) Type II myosin heavy chain  
558 encoded by the *myo2* gene composes the contractile ring during cytokinesis in  
559 *Schizosaccharomyces pombe*. *J Cell Biol* 137(6):1309–1319.
- 560 9. Bi E, et al. (1998) Involvement of an actomyosin contractile ring in *Saccharomyces*  
561 *cerevisiae* cytokinesis. *J Cell Biol* 142(5):1301–1312.
- 562 10. Lippincott J, Li R (1998) Sequential assembly of myosin II, an IQGAP-like protein,  
563 and filamentous actin to a ring structure involved in budding yeast cytokinesis. *J*  
564 *Cell Biol* 140(2):355–366.
- 565 11. Mishra M, et al. (2013) In vitro contraction of cytokinetic ring depends on myosin II  
566 but not on actin dynamics. *Nat Cell Biol*. doi:10.1038/ncb2781.
- 567 12. Mabuchi I, Okuno M (1977) The effect of myosin antibody on the division of  
568 starfish blastomeres. *J Cell Biol* 74(1):251–263.
- 569 13. Mabuchi I (1994) Cleavage furrow: timing of emergence of contractile ring actin  
570 filaments and establishment of the contractile ring by filament bundling in sea  
571 urchin eggs. *J Cell Sci* 107 (7):1853–1862.
- 572 14. Kiehart DP, Mabuchi I, Inoué S (1982) Evidence that myosin does not contribute to  
573 force production in chromosome movement. *J Cell Biol* 94(1):165–178.

- 574 15. O'Connell CB, Warner AK, Wang Y-L (2001) Distinct roles of the equatorial and  
575 polar cortices in the cleavage of adherent cells. *Current Biology* 11(9):702–707.
- 576 16. Wang Y-L (2005) The mechanism of cortical ingression during early cytokinesis:  
577 thinking beyond the contractile ring hypothesis. *Trends Cell Biol* 15(11):581–588.
- 578 17. Kanada M, Nagasaki A, Uyeda TQP (2005) Adhesion-dependent and contractile  
579 ring-independent equatorial furrowing during cytokinesis in mammalian cells. *Mol*  
580 *Biol Cell* 16(8):3865–3872.
- 581 18. Ma X, et al. (2012) Nonmuscle myosin II exerts tension but does not translocate  
582 actin in vertebrate cytokinesis. *Proc Natl Acad Sci USA* 109(12):4509–4514.
- 583 19. De Lozanne A, Spudich JA (1987) Disruption of the *Dictyostelium* myosin heavy  
584 chain gene by homologous recombination. *Science* 236(4805):1086–1091.
- 585 20. Neujahr R, Heizer C, Gerisch G (1997) Myosin II-independent processes in mitotic  
586 cells of *Dictyostelium discoideum*: redistribution of the nuclei, re-arrangement of the  
587 actin system and formation of the cleavage furrow. *J Cell Sci* 110(2):123–137.
- 588 21. Gerisch G, Weber I (2000) Cytokinesis without myosin II. *Curr Opin Cell Biol*  
589 12(1):126–132.
- 590 22. Nagasaki A, de Hostos EL, Uyeda TQP (2002) Genetic and morphological evidence  
591 for two parallel pathways of cell-cycle-coupled cytokinesis in *Dictyostelium*. *J Cell*  
592 *Sci* 115(10):2241–2251.
- 593 23. Lord M, Laves E, Pollard TD (2005) Cytokinesis depends on the motor domains of  
594 myosin-II in fission yeast but not in budding yeast. *Mol Biol Cell* 16(11):5346–5355.
- 595 24. Fang X, et al. (2010) Biphasic targeting and cleavage furrow ingression directed by  
596 the tail of a myosin II. *J Cell Biol* 191(7):1333–1350.
- 597 25. Proctor SA, Minc N, Boudaoud A, Chang F (2012) Contributions of turgor pressure,  
598 the contractile ring, and septum assembly to forces in cytokinesis in fission yeast.  
599 *Current Biology* 22(17):1601–1608.
- 600 26. Jürgens G (2005) Plant cytokinesis: fission by fusion. *Trends Cell Biol* 15(5):277–  
601 283.
- 602 27. Otegui MS, Verbrugghe KJ, Skop AR (2005) Midbodies and phragmoplasts:  
603 analogous structures involved in cytokinesis. *Trends Cell Biol* 15(8):404–413.
- 604 28. McMichael CM, Bednarek SY (2013) Cytoskeletal and membrane dynamics during  
605 higher plant cytokinesis. *New Phytol* 197(4):1039–1057.
- 606 29. Smertenko A, et al. (2017) Plant cytokinesis: terminology for structures and  
607 processes. *Trends Cell Biol* 27(12):885–894.

- 608 30. Johnson UG, Porter KR (1968) Fine structure of cell division in *Chlamydomonas*  
609 *reinhardi* basal bodies and microtubules. *J Cell Biol* 38(2):403–425.
- 610 31. Oakley BR, Bisalputra T (1977) Mitosis and cell division in *Cryptomonas*  
611 (Cryptophyceae). *Can J Botany* 55(22):2789–2800.
- 612 32. Wordeman L, Cande WZ (1990) Cytokinesis by furrowing in diatoms. *Ann N Y*  
613 *Acad Sci* 582:252–259.
- 614 33. Goto Y, Ueda K (1988) Microfilament bundles of F-actin in *Spirogyra* observed by  
615 fluorescence microscopy. *Planta* 173(4):442–446.
- 616 34. Takahashi H, et al. (1998) A possible role for actin dots in the formation of the  
617 contractile ring in the ultra-micro alga *Cyanidium caldarium* RK-1. *Protoplasma*  
618 202:91–104.
- 619 35. Pickett-Heaps JD, Gunning BES, Brown RC, Lemmon BE, Cleary AL (1999) The  
620 cytoplasm concept in dividing plant cells: cytoplasmic domains and the evolution of  
621 spatially organized cell division. *Am J Bot* 86(2):153–172.
- 622 36. Bisgrove SR, Kropf DL (2004) Cytokinesis in brown algae: studies of asymmetric  
623 division in fucoid zygotes. *Protoplasma* 223(2-4):163–173.
- 624 37. Sehring IM, Reiner C, Mansfeld J, Plattner H, Kissmehl R (2007) A broad spectrum  
625 of actin paralogs in *Paramecium tetraurelia* cells display differential localization  
626 and function. *J Cell Sci* 120(Pt 1):177–190.
- 627 38. Paredez AR, et al. (2011) An actin cytoskeleton with evolutionarily conserved  
628 functions in the absence of canonical actin-binding proteins. *Proc Natl Acad Sci*  
629 *USA* 108(15):6151–6156.
- 630 39. Shimizu Y, Kushida Y, Kiriya S, Nakano K, Numata O (2013) Formation and  
631 ingression of division furrow can progress under the inhibitory condition of actin  
632 polymerization in ciliate *Tetrahymena pyriformis*. *Zool Sci* 30(12):1044–1049.
- 633 40. Odrionitz F, Kollmar M (2007) Drawing the tree of eukaryotic life based on the  
634 analysis of 2,269 manually annotated myosins from 328 species. *Genome Biol*  
635 8(9):R196.
- 636 41. Richards TA, Cavalier-Smith T (2005) Myosin domain evolution and the primary  
637 divergence of eukaryotes. *Nature* 436(7054):1113–1118.
- 638 42. Sebé-Pedrós A, Grau-Bové X, Richards TA, Ruiz-Trillo I (2014) Evolution and  
639 classification of myosins, a paneukaryotic whole-genome approach. *Genome Biol*  
640 *Evol* 6(2):290–305.

- 641 43. Cavalier-Smith T, et al. (2014) Multigene eukaryote phylogeny reveals the likely  
642 protozoan ancestors of opisthokonts (animals, fungi, choanozoans) and *Amoebozoa*.  
643 *Molecular Phylogenetics and Evolution* 81:71–85.
- 644 44. Fritz-Laylin LK, et al. (2010) The genome of *Naegleria gruberi* illuminates early  
645 eukaryotic versatility. *Cell* 140(5):631–642.
- 646 45. Brawley SH, Robinson KR (1985) Cytochalasin treatment disrupts the endogenous  
647 currents associated with cell polarization in fucoid zygotes: studies of the role of F-  
648 actin in embryogenesis. *J Cell Biol* 100(4):1173–1184.
- 649 46. Hirono M, et al. (1987) *Tetrahymena* actin: localization and possible biological roles  
650 of actin in *Tetrahymena* cells. *Journal of Biochemistry* 102(3):537–545.
- 651 47. Harper JD, McCurdy DW, Sanders MA, Salisbury JL, John PC (1992) Actin  
652 dynamics during the cell cycle in *Chlamydomonas reinhardtii*. *Cell Motil*  
653 *Cytoskeleton* 22(2):117–126.
- 654 48. Sawitzky H, Grolig F (1995) Phragmoplast of the green alga *Spirogyra* is  
655 functionally distinct from the higher plant phragmoplast. *J Cell Biol* 130(6):1359–  
656 1371.
- 657 49. Varvarigos V, Galatis B, Katsaros C (2005) A unique pattern of F-actin organization  
658 supports cytokinesis in vacuolated cells of *Macrocystis pyrifera* (Phaeophyceae)  
659 gametophytes. *Protoplasma* 226(3-4):241–245.
- 660 50. Traas JA, et al. (1987) An actin network is present in the cytoplasm throughout the  
661 cell cycle of carrot cells and associates with the dividing nucleus. *J Cell Biol*  
662 105(1):387–395.
- 663 51. Higaki T, Kutsuna N, Sano T, Hasezawa S (2008) Quantitative analysis of changes  
664 in actin microfilament contribution to cell plate development in plant cytokinesis.  
665 *BMC Plant Biol* 8(1):80.
- 666 52. Eme L, Moreira D, Talla E, Brochier-Armanet C (2009) A complex cell division  
667 machinery was present in the last common ancestor of eukaryotes. *PLoS ONE*  
668 4(4):e5021.
- 669 53. O'Toole ET, Dutcher SK (2013) Site-specific basal body duplication in  
670 *Chlamydomonas*. *Cytoskeleton*:n/a–n/a.
- 671 54. Ehler LL, Dutcher SK (1998) Pharmacological and genetic evidence for a role of  
672 rootlet and phycoplast microtubules in the positioning and assembly of cleavage  
673 furrows in *Chlamydomonas reinhardtii*. *Cell Motil Cytoskeleton* 40(2):193–207.
- 674 55. Merchant SS, et al. (2007) The *Chlamydomonas* genome reveals the evolution of  
675 key animal and plant functions. *Science* 318(5848):245–250.

- 676 56. Avasthi P, et al. (2014) Actin is required for IFT regulation in *Chlamydomonas*  
677 *reinhardtii*. *Curr Biol* 24(17):2025–2032.
- 678 57. Onishi M, Pringle JR (2016) robust transgene expression from bicistronic mRNA in  
679 the green alga *Chlamydomonas reinhardtii*. *G3 (Bethesda)* 6(12):4115–4125.
- 680 58. Fuhrmann M, Oertel W, Hegemann P (1999) A synthetic gene coding for the green  
681 fluorescent protein (GFP) is a versatile reporter in *Chlamydomonas reinhardtii*.  
682 *Plant J* 19(3):353–361.
- 683 59. Riedl J, et al. (2008) Lifeact: a versatile marker to visualize F-actin. *Nat Methods*  
684 5(7):605–607.
- 685 60. Onishi M, Pringle JR, Cross FR (2016) evidence that an unconventional actin can  
686 provide essential F-actin function and that a surveillance system monitors F-Actin  
687 integrity in *Chlamydomonas*. *Genetics* 202(3):977–996.
- 688 61. Onishi M, Pecani K, Jones T, Pringle JR, Cross FR (2018) F-actin homeostasis  
689 through transcriptional regulation and proteasome-mediated proteolysis. *Proc Natl*  
690 *Acad Sci USA* 115(28):E6487–E6496.
- 691 62. Jack B, Mueller DM, Fee AC, Tetlow AL, Avasthi P (2019) Partially redundant  
692 actin genes in *Chlamydomonas* control transition zone organization and flagellum-  
693 directed traffic. *Cell Reports* 27(8):2459–2467.e3.
- 694 63. Conti MA, Kawamoto S, Adelstein RS (2008) Non-muscle myosin II. *Myosins,*  
695 *Proteins and Cell Regulation*. (Springer, Dordrecht, Dordrecht), pp 223–264.
- 696 64. Kato-Minoura T, Hirono M, Kamiya R (1997) *Chlamydomonas* inner-arm dynein  
697 mutant, *ida5*, has a mutation in an actin-encoding gene. *J Cell Biol* 137(3):649–656.
- 698 65. Hirono M, Uryu S, Ohara A, Kato-Minoura T, Kamiya R (2003) Expression of  
699 conventional and unconventional actins in *Chlamydomonas reinhardtii* upon  
700 deflagellation and sexual adhesion. *Eukaryot Cell* 2(3):486–493.
- 701 66. Zones JM, Blaby IK, Merchant SS, Umen JG (2015) High-resolution profiling of a  
702 synchronized diurnal transcriptome from *Chlamydomonas reinhardtii* reveals  
703 continuous cell and metabolic differentiation. *Plant Cell* 27(10):2743–2769.
- 704 67. Cross FR, Umen JG (2015) The *Chlamydomonas* cell cycle. *Plant J* 82(3):370–392.
- 705 68. Harris JA, Liu Y, Yang P, Kner P, Lehtreck KF (2016) Single-particle imaging  
706 reveals intraflagellar transport-independent transport and accumulation of EB1 in  
707 *Chlamydomonas* flagella. *Mol Biol Cell* 27(2):295–307.
- 708 69. Goodenough UW (1970) Chloroplast division and pyrenoid formation in  
709 *Chlamydomonas reinhardi*. *J Phycol* 6(1):1–6.

- 710 70. Gaffal KP, Arnold CG, Friedrichs GJ, Gemple W (2011) Morphodynamical changes  
711 of the chloroplast of *Chlamydomonas reinhardtii* during the 1st round of division.  
712 *Archiv für Protistenkunde* 145(1-2):10–23.
- 713 71. Harper J, John P (1986) Coordination of division events in the *Chlamydomonas* cell  
714 cycle. *Protoplasma* 131(2):118–130.
- 715 72. Tulin F, Cross FR (2014) A microbial avenue to cell cycle control in the plant  
716 superkingdom. *Plant Cell* 26(10):4019–4038.
- 717 73. Pollard LW, Onishi M, Pringle JR, Lord M (2012) Fission yeast Cyk3p is a  
718 transglutaminase-like protein that participates in cytokinesis and cell morphogenesis.  
719 *Mol Biol Cell* 23(13):2433–2444.
- 720 74. Okada H, Wloka C, Wu J-Q, Bi E (2019) Distinct roles of myosin-ii isoforms in  
721 cytokinesis under normal and stressed conditions. *iScience* 14:69–87.
- 722 75. Calvert MEK, et al. (2011) Myosin concentration underlies cell size-dependent  
723 scalability of actomyosin ring constriction. *J Cell Biol* 195(5):799–813.
- 724 76. Field CM (2005) Characterization of anillin mutants reveals essential roles in septin  
725 localization and plasma membrane integrity. *Development* 132(12):2849–2860.
- 726 77. Kanada M, Nagasaki A, Uyeda TQP (2008) Novel functions of Ect2 in polar  
727 lamellipodia formation and polarity maintenance during “contractile ring-  
728 independent” cytokinesis in adherent cells. *Mol Biol Cell* 19(1):8–16.
- 729 78. Beach JR, Licate LS, Crish JF, Egelhoff TT (2011) Analysis of the role of  
730 Ser1/Ser2/Thr9 phosphorylation on myosin II assembly and function in live cells.  
731 *BMC Cell Biology* 2008 9:55 12(1):52.
- 732 79. Wagner E, Glotzer M (2016) Local RhoA activation induces cytokinetic furrows  
733 independent of spindle position and cell cycle stage. *J Cell Biol* 213(6):641–649.
- 734 80. Kato-Minoura T, Uryu S, Hirono M, Kamiya R (1998) Highly divergent actin  
735 expressed in a *Chlamydomonas* mutant lacking the conventional actin gene.  
736 *Biochem Biophys Res Commun* 251(1):71–76.
- 737 81. Mita T, Kuroiwa T (1988) Division of plastids by a plastid-dividing ring in  
738 *Cyanidium caldarium*. *Cell Dynamics* (Springer, Vienna), pp 133–152.
- 739 82. Hashimoto H (1992) Involvement of actin filaments in chloroplast division of the  
740 alga *Closterium ehrenbergii*. *Protoplasma* 167(1-2):88–96.
- 741 83. Sumiya N, Fujiwara T, Era A, Miyagishima S-Y (2016) Chloroplast division  
742 checkpoint in eukaryotic algae. *Proc Natl Acad Sci USA* 113(47):E7629–E7638.

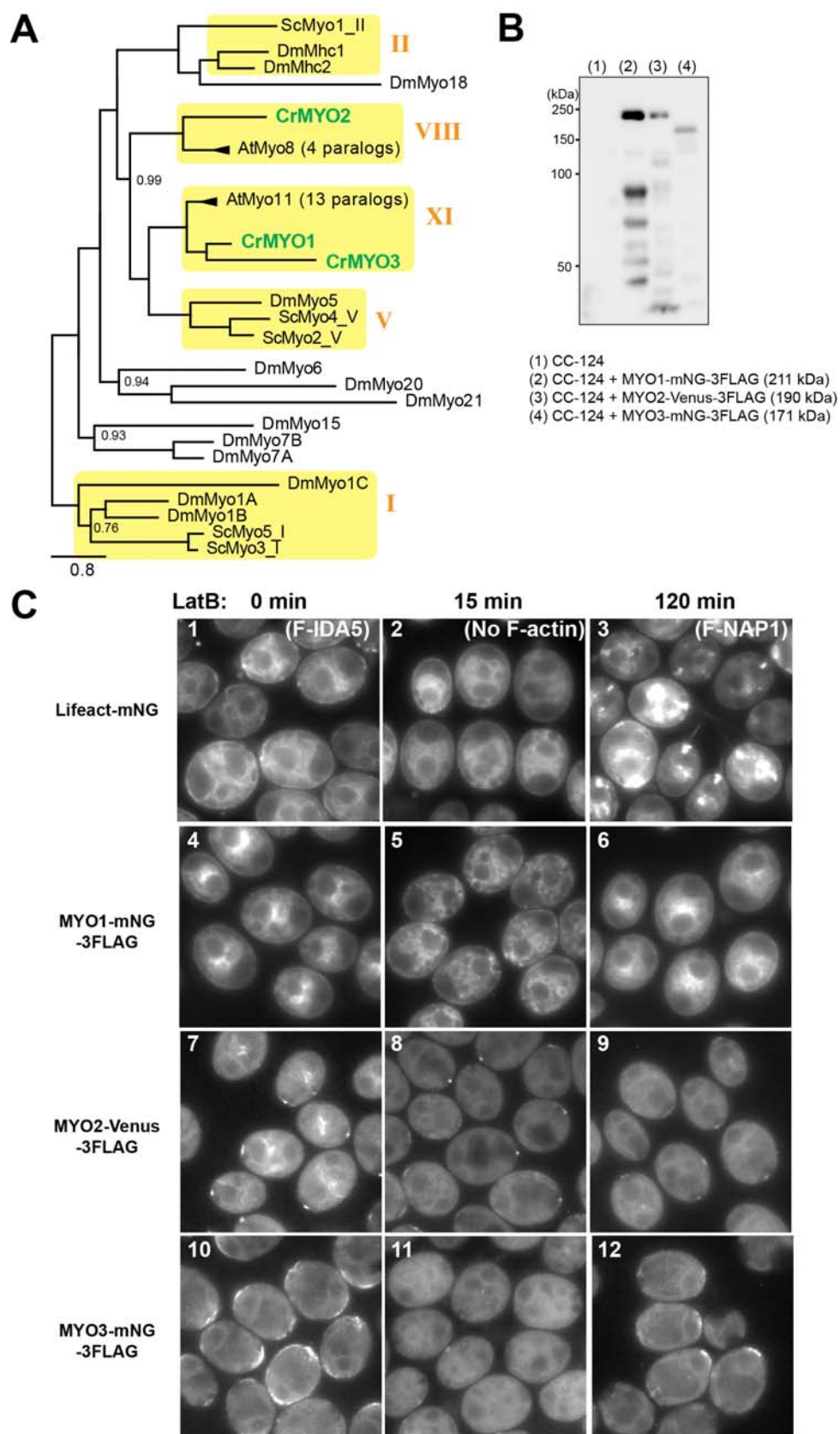


- 743 84. Miyagishima S-Y, Suzuki K, Okazaki K, Kabeya Y (2012) Expression of the  
744 nucleus-encoded chloroplast division genes and proteins regulated by the algal cell  
745 cycle. *Molecular Biology and Evolution* 29(10):2957–2970.
- 746 85. Doonan JH, Grief C (1987) Microtubule cycle in *Chlamydomonas reinhardtii*: An  
747 Immunofluorescence study. *Cell Motil Cytoskeleton* 7(4):381–392.
- 748 86. Gaffal KP, el-Gammal S (1990) Elucidation of the enigma of the “metaphase band”  
749 of *Chlamydomonas reinhardtii*. *Protoplasma* 156:139–148.
- 750 87. Carvalho A, Desai A, Oegema K (2009) Structural memory in the contractile ring  
751 makes the duration of cytokinesis independent of cell size. *Cell* 137(5):926–937.
- 752 88. Davies T, et al. (2018) Cell-intrinsic and -extrinsic mechanisms promote cell-type-  
753 specific cytokinetic diversity. *eLife Sciences* 7:113.
- 754 89. Hardin WR, et al. (2017) Myosin-independent cytokinesis in *Giardia* utilizes  
755 flagella to coordinate force generation and direct membrane trafficking. *Proc Natl*  
756 *Acad Sci USA* 114(29):E5854–E5863.
- 757 90. Matsuzaki M, et al. (2004) Genome sequence of the ultrasmall unicellular red alga  
758 *Cyanidioschyzon merolae* 10D. *Nature* 428(6983):653–657.
- 759 91. Bi E, Lutkenhaus J (1991) FtsZ ring structure associated with division in  
760 *Escherichia coli*. 354(6349):161–164.
- 761 92. Margolin W (2005) FtsZ and the division of prokaryotic cells and organelles. *Nat*  
762 *Rev Mol Cell Biol* 6(11):862–871.
- 763 93. Osawa M, Anderson DE, Erickson HP (2008) Reconstitution of contractile FtsZ  
764 rings in liposomes. *Science* 320(5877):792–794.
- 765 94. Bisson-Filho AW, et al. (2017) Treadmilling by FtsZ filaments drives peptidoglycan  
766 synthesis and bacterial cell division. *Science* 355(6326):739–743.
- 767 95. Yang X, et al. (2017) GTPase activity–coupled treadmilling of the bacterial tubulin  
768 FtsZ organizes septal cell wall synthesis. *Science* 355(6326):744–747.
- 769 96. Balasubramanian MK, Srinivasan R, Huang Y, Ng K-H (2012) Comparing  
770 contractile apparatus-driven cytokinesis mechanisms across kingdoms. *Cytoskeleton*  
771 (*Hoboken*) 69(11):942–956.
- 772 97. Lindås A-C, Karlsson EA, Lindgren MT, Ettema TJG, Bernander R (2008) A unique  
773 cell division machinery in the Archaea. *Proc Natl Acad Sci USA* 105(48):18942–  
774 18946.
- 775 98. Zaremba-Niedzwiedzka K, et al. (2017) Asgard archaea illuminate the origin of  
776 eukaryotic cellular complexity. *Nature* 541(7637):353–358.

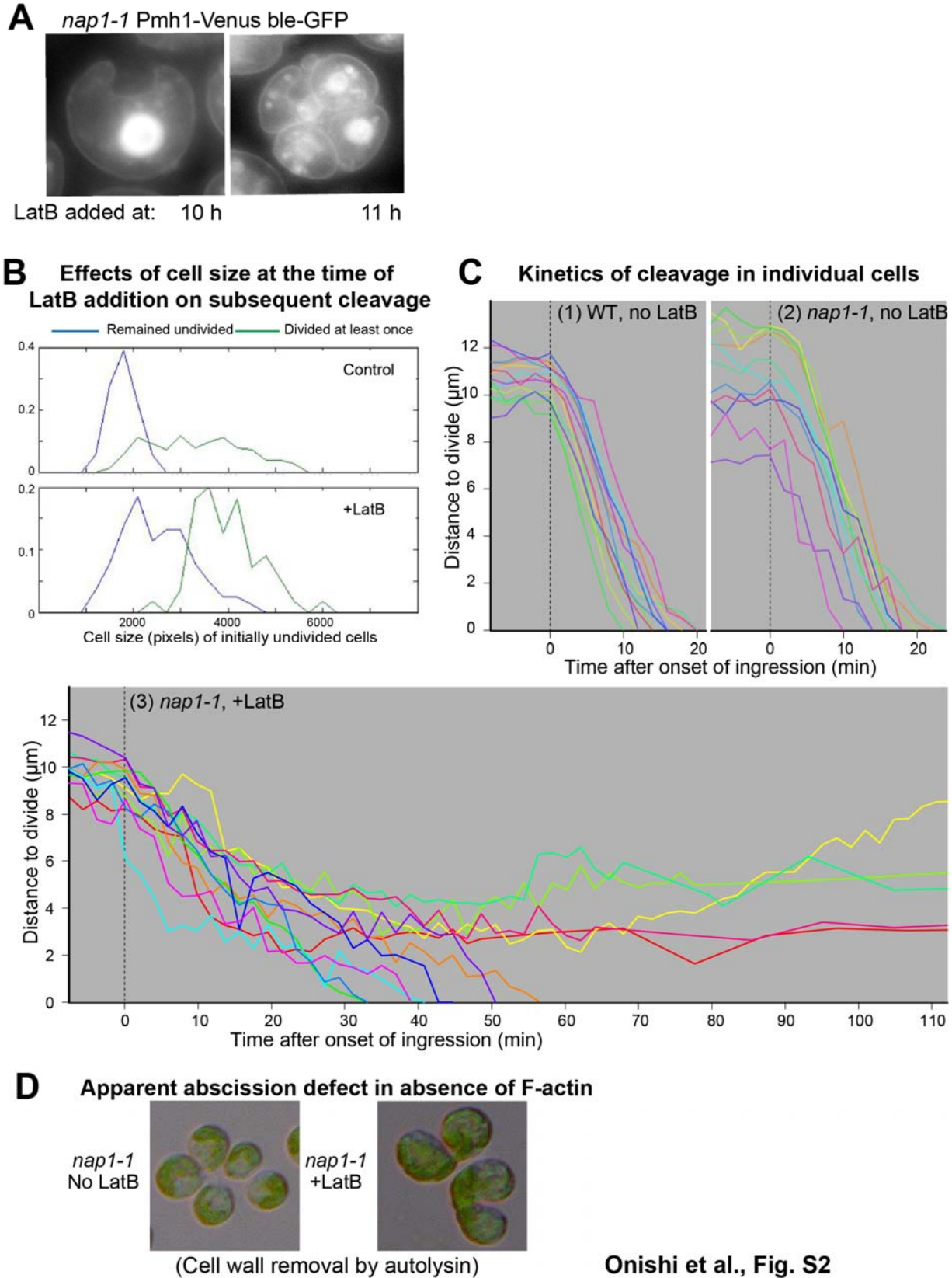


- 777 99. 1. Duggin IG, et al. (2015) CetZ tubulin-like proteins control archaeal cell shape.  
778 *Nature* 519(7543):362–365.
- 779 100. Walsh JC, et al. (2019) Division plane placement in pleomorphic archaea is  
780 dynamically coupled to cell shape. *Mol Microbiol* 112(3):785–799.
- 781 101. Erickson HP (2009) Modeling the physics of FtsZ assembly and force generation.  
782 *Proc Natl Acad Sci USA* 106(23):9238–9243.
- 783 102. Ochs J, LaRue T, Tinaz B, Yongue C, Domozych DS (2014) The cortical  
784 cytoskeletal network and cell-wall dynamics in the unicellular charophycean green  
785 alga *Penium margaritaceum*. *Ann Bot* 114(6):1237–1249.
- 786 103. Farr H, Gull K (2012) Cytokinesis in trypanosomes. *Cytoskeleton (Hoboken)*  
787 69(11):931–941.
- 788 104. Brown JM, Marsala C, Kosoy R, Gaertig J (1999) Kinesin-II is preferentially  
789 targeted to assembling cilia and is required for ciliogenesis and normal cytokinesis  
790 in *Tetrahymena*. *Mol Biol Cell* 10(10):3081–3096.
- 791 105. Shaw MK, Compton HL, Roos DS, Tilney LG (2000) Microtubules, but not actin  
792 filaments, drive daughter cell budding and cell division in *Toxoplasma gondii*. *J Cell*  
793 *Sci* 113 ( Pt 7):1241–1254.
- 794 106. Danilchik MV, Funk WC, Brown EE, Larkin K (1998) Requirement for  
795 microtubules in new membrane formation during cytokinesis of *Xenopus* embryos.  
796 *Dev Biol* 194(1):47–60.
- 797 107. Danilchik MV, Bedrick SD, Brown EE, Ray K (2003) Furrow microtubules and  
798 localized exocytosis in cleaving *Xenopus laevis* embryos. *J Cell Sci* 116(2):273–283.
- 799 108. Jesuthasan S (1998) Furrow-associated microtubule arrays are required for the  
800 cohesion of zebrafish blastomeres following cytokinesis. *J Cell Sci* 111(24):3695–  
801 3703.
- 802 109. Albertson R, Cao J, Hsieh T-S, Sullivan W (2008) Vesicles and actin are targeted to  
803 the cleavage furrow via furrow microtubules and the central spindle. *J Cell Biol*  
804 181(5):777–790.
- 805 110. van den Ent F, Amos LA, Löwe J (2001) Prokaryotic origin of the actin cytoskeleton.  
806 *Nature* 413(6851):39–44.
- 807 111. Lindås A-C, Valegård K, Ettema TJG (2017) Archaeal actin-family filament  
808 systems. *Subcell Biochem* 84(8):379–392.
- 809 112. Ettema TJG, Lindås A-C, Bernander R (2011) An actin-based cytoskeleton in  
810 archaea. *Mol Microbiol* 80(4):1052–1061.

- 811 113. Buschmann H, Zachgo S (2016) The evolution of cell division: From Streptophyte  
812 algae to land plants. *Trends in Plant Science* 21(10):872–883.
- 813 114. Li Y, Liu D, López-Paz C, Olson BJ, Umen JG (2016) A new class of cyclin  
814 dependent kinase in *Chlamydomonas* is required for coupling cell size to cell  
815 division. *eLife Sciences* 5. doi:10.7554/eLife.10767.
- 816 115. Gorman DS, Levine RP (1965) Cytochrome f and plastocyanin: their sequence in  
817 the photosynthetic electron transport chain of *Chlamydomonas reinhardi*. *Proc Natl*  
818 *Acad Sci USA* 54(6):1665–1669.
- 819 116. Dutcher SK (1995) Mating and tetrad analysis in *Chlamydomonas reinhardtii*.  
820 *Methods Cell Biol* 47:531–540.
- 821 117. Tulin F (2019) Mating and tetrad dissection in *Chlamydomonas*. *Bio Protoc* 9(7).  
822 doi:10.21769/BioProtoc.3207.
- 823 118. Gibson DG, et al. (2009) Enzymatic assembly of DNA molecules up to several  
824 hundred kilobases. *Nat Methods* 6(5):343–345.
- 825 119. Fang S-C, de los Reyes C, Umen JG (2006) Cell size checkpoint control by the  
826 retinoblastoma tumor suppressor pathway. *PLoS Genet* 2(10):e167.
- 827 120. Tulin F, Cross FR (2015) Cyclin-dependent kinase regulation of diurnal  
828 transcription in *Chlamydomonas*. *Plant Cell* 27(10):2727–2742.
- 829 121. Atkins KC, Cross FR (2018) Interregulation of CDKA/CDK1 and the plant-specific  
830 cyclin-dependent kinase CDKB in control of the *Chlamydomonas* cell cycle. *Plant*  
831 *Cell* 30(2):429–446.
- 832 122. Dutcher SK (1995) Purification of basal bodies and basal body complexes from  
833 *Chlamydomonas reinhardtii*. *Methods Cell Biol* 47:323–334.
- 834 123. Guindon S, et al. (2010) New algorithms and methods to estimate maximum-  
835 likelihood phylogenies: assessing the performance of PhyML 3.0. *Syst Biol*  
836 59(3):307–321.
- 837 124. Lupas A, Van Dyke M, Stock J (1991) Predicting coiled coils from protein  
838 sequences. *Science* 252(5009):1162–1164.
- 839



841 **Fig. S1.** (A) Maximum-likelihood tree of amino-acid sequences of all myosins from *D. melanogaster* (Dm), *S.*  
842 *cerevisiae* (Sc), *A. thaliana* (At), and *C. reinhardtii* (Cr). Three *Chlamydomonas* myosins (green) clustered  
843 with plant-specific type-VIII and type-XI myosins. Scale bar, substitutions per residue. Branch supports  
844 below 1 are shown next to nodes. See Materials and Methods for details. (B) Expression of mNG-3FLAG-  
845 tagged or Venus-3-FLAG-tagged myosins. Whole-cell extracts from wild-type (CC-124) and transformed  
846 cells were analyzed by Western blotting using an anti-FLAG antibody. The positions of molecular-weight  
847 markers and the predicted molecular weights of the tagged proteins are indicated. (C) Response of F-actin and  
848 the tagged myosins to LatB treatment. Cells expressing Lifeact-mNG (1-3) or a tagged myosin (4-12) were  
849 treated with 10  $\mu$ M LatB for the indicated times. See text for details.



850

851 **Fig. S2.** (A) Failure of mitosis when F-actin is eliminated sufficiently early in the cell cycle. In an experiment

Onishi et al., Fig. S2

852 like that of Fig. 4A, *nap1-1* cells expressing PMH1-Venus and the nuclear marker ble-GFP were treated with 3  
853  $\mu$ M LatB beginning at the indicated times and imaged at 20 h. (B) Correlation between cell size and successful  
854 formation of furrows in the absence of F-actin. *nap1-1* cells were synchronized using the -N method (see  
855 Materials and Methods). At 11 hr, as cells began to enter divisions, they were transferred to fresh plates with  
856 or without 3  $\mu$ M LatB and imaged every 30 minutes by brightfield time-lapse microscopy. The fractions of  
857 initially undivided cells that divided successfully were plotted as a function of the size of the cells at the time  
858 of transfer. (C) The kinetics of cleavage in individual cells in the experiments of Fig. 5. (D) Additional  
859 evidence for an abscission defect in cells lacking F-actin. In the experiment of Fig. 4A, control cells and cells  
860 treated with LatB beginning at 11 h were examined at 20 h. Cells were treated with autolysin before  
861 examination (see Materials and Methods). Control cells became rounder than normal as a result of cell-wall  
862 removal. ~5% of the LatB-treated cells remained connected by narrow intercellular bridges.